O'Connor, L. K., Robinson, S. A., Naafs, B. D. A., Jenkyns, H. C., Henson, S., Clarke, M., & Pancost, R. D. (2019). Late Cretaceous Temperature Evolution of the Southern High Latitudes: A TEX_{86} Perspective . *Paleoceanography and Paleoclimatology*, *34*(4), 436-454. https://doi.org/10.1029/2018PA003546

Late Cretaceous temperature evolution of the southern high latitudes: a TEX_{86} perspective

Lauren K. O'Connor[1*], Stuart A. Robinson[1], B. David A. Naafs[2], Hugh C. Jenkyns[1], Sam Henson[1], Madeleine Clarke[3], Richard D. Pancost[2]

[1]Department of Earth Sciences, University of Oxford, South Parks Road, Oxford, OX1 3AN, UK. [2]Organic Geochemistry Unit, School of Earth Sciences and School of Chemistry, University of Bristol, Bristol BS8 1RJ, UK. [3]Department of Earth Sciences, University College London, Gower Street, London, WC1E 6BT, UK.

Corresponding author: Lauren O'Connor (lauren.oconnor@earth.ox.ac.uk)

Key Points:

- New TEX_{86} data show extreme warmth in the southern high-latitudes during the Late Cretaceous
- These data indicate slow, steady cooling from the Turonian–mid-Campanian

Abstract

The Late Cretaceous was a greenhouse world, characterized by elevated temperatures and high atmospheric pCO_2. However, even in the context of an extreme greenhouse climate, existing planktic foraminiferal $\delta^{18}O$ data from the Falkland Plateau (paleolatitude of ~55˚S) suggest anomalous warmth, with sea-surface temperatures (SSTs) >30°C for much of the Late Cretaceous, followed by cooling. Over the last two decades there has been discussion as to whether these high $\delta^{18}O$-based SSTs reflect a genuine temperature signal and, if so, whether there was a local temperature anomaly in the South Atlantic or whether the data are representative of zonal paleotemperatures at 55˚S. To provide new insights into the degree of ocean warming in the southern high-latitudes during the Late Cretaceous (Cenomanian to Campanian), new SST records from the Falkland and Kerguelen Plateaus are presented here using the organic geochemical paleothermometer TEX_{86}. Overall, the TEX_{86} data support the $\delta^{18}O$ data, indicating extreme and widespread warmth in the mid- to high southern latitudes in the Late Cretaceous, with SSTs from 27–37°C. Crucially, the TEX_{86} data show slow, steady cooling from the Turonian to the Campanian, and suggest that temperature gradients during the Campanian did not become as steep as suggested by some planktic foraminiferal data.

1 Introduction

The Late Cretaceous (100.5-66.0 Ma) was a greenhouse world, characterized by high temperatures and reduced latitudinal temperature gradients (Sinninghe Damsté et al., 2010; O'Brien et al., 2017; Robinson et al., 2019). Peak warmth was attained in the Cenomanian–Turonian (~100-90 Ma) (Jenkyns et al., 1994; Norris & Wilson, 1998; Clarke & Jenkyns, 1999;

Wilson & Norris, 2001; Norris et al., 2002; Wilson et al., 2002; Voigt et al., 2004; Forster et al., 2007) with sea-surface temperatures (SSTs) reaching ≥ 30°C in the tropics and the southern mid- to high-latitudes (Huber et al., 1995, 2002, 2018; Bice et al., 2003, 2006; MacLeod et al., 2013; O'Brien et al., 2017; Robinson et al., 2019). After this interval, sea-surface and deep-water temperatures decreased to the cooler greenhouse of the Campanian–Maastrichtian (80-66 Ma) (Huber et al., 1995, 2002, 2018; MacLeod et al., 2005; Friedrich et al., 2012; Linnert et al., 2014; O'Brien et al., 2017).

However, even in the context of an extreme greenhouse climate, $\delta^{18}O$ data from some parts of the Southern Hemisphere show anomalous warmth: in particular, estimates from Sites 327 and 511 at the Falkland Plateau (Figure 1) suggest that, at paleolatitudes of ~55–60˚S, SSTs exceeded 30°C for much of the Late Cretaceous, before cooling rapidly in the mid-Campanian (Huber et al., 1995, 2018; Bice et al., 2003). By contrast, modern mean annual SSTs at ~60°S are ~0°C (NOAA 2013). If these records from Falkland Plateau are indicative of widespread and prolonged warmth in the mid- to high-latitudes, there are major implications for polar climate and latitudinal temperature gradients in a greenhouse world. These high temperatures within 15 to 20˚ latitude of the coast of Antarctica question the feasibility of polar ice caps and sea-ice during the Late Cretaceous (cf. Price, 1999; Li et al., 2000; Gale et al., 2002; Miller et al., 2003, 2005; Bornemann et al., 2008; Davies et al., 2009; Galeotti et al., 2009; Bowman et al., 2013). In addition, the high $\delta^{18}O$-based temperatures are not easily reconciled with climate models without extremely high atmospheric pCO_2 (≥3000 ppm; e.g. Poulsen et al., 1999; Bice et al., 2003, 2006). Such high pCO_2 values are not corroborated by most proxy or carbon-cycle models for the Late Cretaceous (reviewed in Foster et al., 2017).

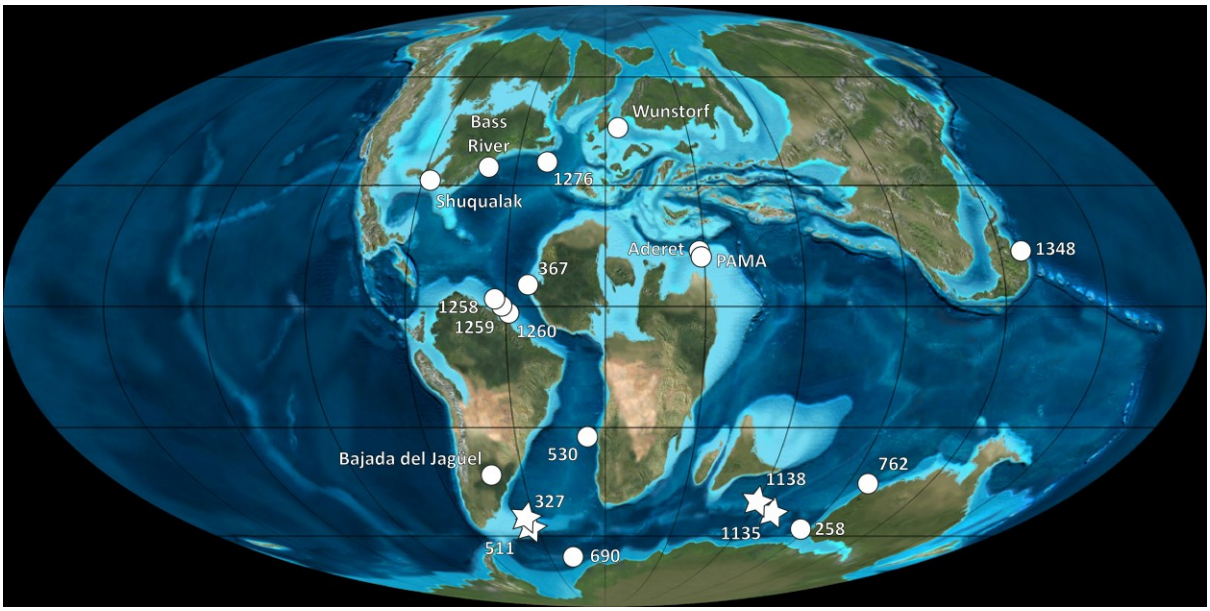

Figure 1. DSDP/ODP/IODP Sites used in this study (stars) and previously published data (circles). Base map shows late Turonian (90 Ma) paleogeography (adapted from Blakey 2016).

Considering these issues, the $\delta^{18}O$ values might not purely reflect temperature but could be, at least in part, an artefact of diagenetic alteration or depletion of local $\delta^{18}O_{sw}$. Diagenetic alteration at Sites 327 and 511 was deemed unlikely based on the high quality of preservation of the foraminifera and the separation between planktic and benthic values, which suggests no post-mortem calcification (Huber et al., 1995, 2018; Bice et al., 2003). Factors leading to the isotopic depletion of local seawater have been similarly eliminated: there is no evidence for a drastic increase in freshwater flux to the surface ocean nor any means of sufficiently depleting the surface waters to cause such light $\delta^{18}O$ values (Bice et al., 2003). Further, new foraminiferal $\delta^{18}O$ data from the southern Indian Ocean (DSDP Site 258) spanning the Cenomanian–Campanian interval corroborate the isotopically light values reported for the Falkland Plateau (Huber et al., 2018). Nonetheless, a long-standing question in paleoceanography is whether the

high $\delta^{18}O$-based sea-surface temperatures from the Falkland Plateau in the Late Cretaceous reflect a genuine temperature signal and, if so, is this simply a local anomaly or a more widespread feature of the climate at this time?

Here, we explore this question using an independent SST proxy: the organic paleothermometer TEX_{86} (TetraEther indeX of 86 carbon atoms) applied to sediments from sites at the Falkland and Kerguelen Plateaus (in the southern Atlantic and Indian Oceans, respectively) spanning the Late Cretaceous interval. Based on the relationship between the distribution of archaeal membrane lipids (glycerol dialkyl glycerol tetraethers—GDGTs) in marine core-top sediments and SST (Schouten et al., 2002, 2003, 2013), TEX_{86} has been used extensively to reconstruct SSTs during the Cretaceous (e.g. Littler et al., 2011; Naafs & Pancost, 2016; O'Brien et al., 2017; Robinson et al, 2019). Through assessing potential influences on both TEX_{86} and foraminiferal $\delta^{18}O$ values, and employing a multi-proxy approach, this study investigates the temperature evolution of the Falkland and Kerguelen Plateaus during the Late Cretaceous.

2 Study areas

2.1 Falkland Plateau

Samples are used from Deep Sea Drilling Project (DSDP) Sites 327 and 511 from the Falkland Plateau (Figure 1), which is a submarine projection of the South American continental margin, extending 1800 km east of the Falkland Islands. The Falkland Plateau broke away from southern Africa during the Aptian–Albian interval and, after final separation, subsided rapidly, reaching bathyal depths sometime during the late Albian–Cenomanian (Krasheninnikov & Basov, 1983). By the late Aptian, the Plateau was relatively isolated from the influence of

continental runoff from Africa (Thompson 1977), and terrigenous sediment supply from the Andean cordillera probably slowed after the mid-Cretaceous Andean orogeny (Barker et al., 1977a). Deposition of organic-rich black shales under anoxic conditions typified the mid- to Late Jurassic but more open-marine environments with well-oxygenated sea floors and pelagic sedimentation was established on the Plateau by the early to middle Albian (Thompson, 1977). A deep connection developed between the Atlantic and Indian Oceans in the mid-Cretaceous, with an increase in Atlantic deep-water formation driving improved circulation and ventilation during the Late Cretaceous as the plateau continued to subside (Barker et al., 1977b; Robinson et al., 2010; Robinson & Vance, 2012). Paleogeographic reconstructions indicate that Sites 327 and 511 lay between ~55 and ~60°S during the Late Cretaceous (e.g. Huber et al., 1995; Hay et al., 1999; Van Hinsbergen et al., 2015). The age models developed by Huber et al. (2018) are used for both sites.

Site 327 is currently located at 50.5°S, 46.5°W on the Maurice Ewing Bank in the Falkland Plateau Basin, ~10 km northeast of Site 511. Only the Campanian section is used in this study (90–142 mbsf), which comprises 52 m of greenish-grey calcareous ooze (Barker et al., 1977b, 1977c). Foraminifera are abundant in the Campanian section, with high planktic to benthic ratios and excellent preservation, indicating deposition above the foraminiferal lysocline in a lower bathyal environment at that time (Basov and Krasheninnikov, 1983).

Site 511 is currently located at 51.0 °S, 47.6 °W in the basin province of the Falkland Plateau. The Turonian to Campanian section (~200–430 mbsf) is used in this study and comprises pale grey calcareous ooze and zeolitic foraminiferal ooze, and grey zeolitic clay and claystone (Ludwig et al., 1983). In general, the occurrence of planktic foraminifers in the Upper Cretaceous sediments is quite sporadic but, in sections with abundant foraminifera, preservation

is described as "excellent" (Huber et al., 1995), possibly owing to shallow burial depths and high clay content. Sedimentation at this site was highly episodic, with episodes of exceptionally high sedimentation rates separated by condensed intervals or hiatuses (Ludwig et al., 1983).

2.2 Kerguelen Plateau

In addition to samples from the Falkland Plateau, samples used in this study derive from Ocean Drilling Program (ODP) Sites 1138 and 1135 located on the Kerguelen Plateau (Figure 1). This plateau is a submarine Large Igneous Province, generated by the Kerguelen hot spot in the Early Cretaceous (Frey et al., 2000). Formed ~100 Mya on the Antarctic Plate, the Kerguelen Plateau has remained at a relatively constant paleolatitude of ~50–60°S since its formation, recording a transition from shallow-marine to deeper marine deposition throughout the Late Cretaceous (Meyers et al., 2009; Dickson et al., 2017).

Site 1135 is located at 59.4°S, 84.2°E on the Southern Kerguelen Province. Samples used here are of Cenomanian–Maastrichtian age (~260–530 mbsf) and comprise a sequence of white to light greenish-grey calcareous ooze and chalk (Coffin et al., 2000; Petrizzo, 2001).

Site 1138 is located at 53.3°S, 75.6°E on the Central Kerguelen Province. The samples used here are of Cenomanian–Maastrichtian age (~480–660 mbsf), and the sequence consists of cyclic alternations of white foraminifer-bearing chalk and grey to greenish grey to black intervals of nannofossil claystone (Coffin et al., 2000; Mohr et al., 2002; Dickson et al., 2017). The base of the sequence contains an organic-rich claystone (<20% TOC), indicative of low-oxygen conditions, thought to represent OAE 2 and record the Cenomanian–Turonian Boundary (Meyers et al., 2009, Dickson et al., 2017). Some TEX_{86} data have been published by Robinson et al. (2019) from around the Cenomanian–Turonian boundary and these data are integrated with new data from the Turonian–Santonian sediments.

Detailed foraminiferal biostratigraphy for the Turonian–Santonian at both sites (Petrizzo, 2001) and nannofossil biostratigraphy for the Cenomanian–Campanian at Site 1138 (Russo, 2014) allows correlation of the Kerguelen Plateau section with other localities. Age models for both sites have been constructed based upon combined carbon-isotope and biostratigraphy (see supplementary information for details).

3. Methods

3.1 Organic geochemistry

All samples were oven-dried overnight at 40°C to remove residual water and the edges were scraped clean using a metal spatula to remove any loose rock debris or other detritus, before being finely ground and homogenized.

The Total Lipid Extract (TLE) was obtained via solvent extraction, using either an ultrasonic bath (method described in Linnert et al., 2014) at University College London (UCL) or using an Analytix Advanced Microwave Digestion System at the University of Oxford. For the latter method, lipids were solvent-extracted from 5 g of sediment using 20 mL of DCM/methanol (9:1, v/v). Temperature in the microwave was programmed to increase linearly from room temperature to 70 °C over 10 minutes, hold at 70 °C for 10 minutes, and then cool to 25°C over 20 minutes.

At UCL, the TLE was split into polar and apolar fractions before analysis of glycerol dialkyl glycerol tetraethers (GDGTs), following the method described in Linnert et al., (2014). However, due to the low concentrations of organic matter in many of the samples, the TLE extracted at Oxford was not split before GDGT analysis (some samples were split later for analysis of the apolar fractions). Prior to analysis, the TLE (Oxford) or polar (UCL) fraction was

re-dissolved in a hexane-isopropanol mixture (99:1, v/v) and passed through a 0.45 μm polytetrafluoroethylene filter.

Analysis of GDGTs at UCL and Oxford (see supplementary information) followed the methods described in Littler et al. (2011) and Linnert et al. (2014) using an Agilent 1200 series HPLC attached to a G6130A single-quadrupole mass spectrometer (note that the same instrument was used as it was moved from UCL to Oxford). The analytical protocol followed was as described in Schouten et al. (2007). For samples analyzed in Bristol (see supplementary information), GDGTs were analysed using a ThermoFisher Scientific Accela Quantum Access triple quadrupole mass spectrometer at the Organic Geochemistry Unit (University of Bristol). Normal phase separation was achieved using two ultra-high performance liquid chromatography silica columns, following Hopmans et al., (2016). For both sample sets, the isoprenoid and branched GDGT (isoGDGTs and brGDGTS, respectively) abundances were measured in selective ion monitoring (SIM) mode (*m/z* 1302, 1300, 1298, 1296, 1294, 1292, 1050, 1048, 1046, 1036, 1034, 1032, 1022, 1020, 1018, 744, and 653). Ion peaks of the GDGTs were integrated to determine the relative abundance of each compound. The relative abundance of some of the isoGDGTs was used to determine the TEX_{86} (Schouten et al., 2002) value for each sample using the following equation:

$$TEX_{86} = \frac{isoGDGT\_2 + isoGDGT\_3 + cren.isomer}{isoGDGT\_1 + isoGDGT\_2 + isoGDGT\_3 + cren.isomer}$$

In both analytical laboratories (UCL and Bristol), repeated analysis of in-house standards alongside the samples reported here suggests long-term reproducibility of TEX_{86} values of ±0.05 (1σ). Comparison of TEX_{86} values measured in the different laboratories suggests no significant difference between them. Other GDGT-based indices used to determine the reliability of the

TEX_{86} data, e.g. BIT index (Hopmans et al., 2004), Methane Index (MI) (Zhang et al., 2011), %GDGT-0 (Sinninghe Damsté et al., 2012), and the Ring Index (ΔRI) (Zhang et al., 2011) were also calculated where possible using the relative abundances of isoGDGTs and brGDGTs. The BAYSPAR (Tierney & Tingley, 2014, 2015), TEX_{86}^{H} (Kim et al., 2010) and linear (O'Brien et al., 2017) calibrations were used to convert TEX_{86} to SSTs. The relative strengths and weaknesses of these calibrations for Cretaceous SSTs are discussed in O'Brien et al. (2017); we have no preference. Where TEX_{86}- and $\delta^{18}O$-SSTs are compared, the TEX_{86} calibration with the minimum offset is used.

To determine the thermal maturity of the organic matter, the C_{31}-homohopane distribution in representative samples was analyzed (Mackenzie et al., 1980). For this purpose, elemental sulphur was removed from the apolar fractions using activated copper. The apolar fraction was dissolved in 1 mL hexane, to which the activated copper was added until the reaction ceased, then left for 24 hours. These samples were then analyzed using a Finnigan Trace gas chromatograph-mass spectrometer (GC–MS) in the Organic Geochemistry Unit (University of Bristol). The GC oven program was: 70°C (1 min hold) to 130°C at 20°C/min, then to 300°C (held for 24 min) at 4°C/min. Separation was achieved using a Zebron non-polar column (50 m x 0.32 mm, 0.10 µm film thickness). The injection volume was 1 µl. The mass spectrometer continuously scanned between *m/z* 50 and 650. Using the *m/z* 191 trace that is characteristic for hopanes, the relative abundance of the different homologues of the C_{31}-homohopane was quantified as a proxy for thermal maturity (Mackenzie et al., 1980) and constrain its influence on TEX_{86} values (e.g. Schouten et al., 2004).

$$C_{31}\ hopane\ ratio = \frac{\beta\beta}{(\alpha\beta + \beta\alpha + \beta\beta)}$$

3.2 Stable isotope analysis

Samples from DSDP Sites 327 and 511 on the Falkland Plateau were also used for foraminiferal $\delta^{18}O$ analysis. Sediments were left in a beaker of deionised water for several hours until they disaggregated and were then wet-sieved, keeping the ≥63 μm fraction, which was oven-dried at 40°C overnight. For all samples, the best-preserved (glassy) specimens were selected to eliminate any obvious diagenetic influence on isotopic values. Also, the largest specimens were selected and, where possible, all from the same size fraction to minimize artefacts of size- and age-dependent isotopic values. ~20–50 μg of a single species were picked for each analysis (see supplementary information). Samples were crushed prior to analysis, but due to the small size of the samples and the risk of losing sample material, further cleaning was not conducted. Isotope measurements were performed on a Delta V Advantage isotope mass spectrometer fitted with a Kiel IV carbonate device. Oxygen isotope values are reported using the standard delta notation in parts per mil relative to VPDB. Three standards were used: NOCZ, NSB-18, and NSB-19; reproducibility (±1σ) of $\delta^{18}O$ from these standards was 0.08%, 0.03%, and 0.06%, respectively. $\delta^{18}O$ values are expressed in per mil variations relative to VPDB.

Samples from ODP Sites 1135 and 1138 were analyzed for bulk carbonate stable isotopes. Samples were oxidized to remove organic matter; H_2O_2 (15%, pH 8,) was added to each sample and allowed to react for 30 minutes, then oven-dried at 40°C. Measurements were performed on a Delta V Advantage isotope mass spectrometer fitted with a Gas Bench II in the Department of Earth Sciences (University of Oxford); the carbonates were converted to CO_2 with 100% H_3PO_4. Two standards were used: NBS-18 and NBS-19. Repeat analysis of standards gives a standard deviation of 0.03 for $\delta^{18}O$ and 0.03 $\delta^{13}C$, (n=15). $\delta^{18}O$ and $\delta^{13}C$ values are expressed in per mil variations relative to VPDB.

3.3 Rock-Eval

TOC content and %Mineral Carbon data were obtained using the Rock-Eval 6 Standard Analyzer at the Department of Earth Sciences (University of Oxford). ~60 mg of sediment was analyzed in the oxidation and pyrolysis ovens, by heating with incremental temperature increases from room temperature to 850°C. Mineral carbon content was calculated from the S3MINC and S5 peaks, produced from the CO and CO_2 flux from the sample and analysed by infrared detector (Behar et al., 2001). The TOC content was simultaneously obtained from the combined CO and CO_2 fluxes representing the Pyrolyzable Carbon (S1 + S2 + S3CO + $S3CO_2$) and the Residual Carbon (S4CO + $S4CO_2$). An in-house standard was regularly measured every ~10 samples. The reproducibility (±1σ) for TOC and %Mineral Carbon was 0.43% and 0.01% respectively.

4 Results and data interpretation

4.1 Falkland Plateau

4.1.1 DSDP Site 327

16 samples of Campanian age contained quantifiable GDGTs, yielding TEX_{86} values ranging from 0.47–0.78 (Figure 2), corresponding to TEX_{86}-SSTs of 13–34.3°C (BAYSPAR; supplementary information). BIT values range from 0.00 to 0.43, %GDGT-0 from 17 to 82 %, Methane Index from 0.21 to 0.84, and ΔRIs from |0.03| to |1.57| (see supplementary information for methods and data). The samples with high |ΔRI| values also have high MIs and %GDGT-0 values, implying that methanogenesis was the likely cause of anomalous GDGT distributions. Samples with high BIT values may have been influenced by terrestrial-derived GDGTs. After removing samples with unacceptable BIT (≥0.4), %GDGT-0 (≥67%), Methane Index (≥0.5), or Ring Index (≥|0.3|) values, 6 samples remained with TEX_{86} values from 0.47–0.78. These

samples show no discernible stratigraphic trend. T_{max} values were ≤463°C (supplementary information). A C_{31}-hopane ratio was only obtained for one sample, which gave a value of 0.50.

15 samples contained sufficient foraminifera for analysis, 13 of which contained enough for the analysis of two different species. These analyses produced $\delta^{18}O_{pf}$ values of -1.12 to 0.05‰ (Figure 2). $\delta^{18}O_{pf}$ values were converted to paleotemperatures using the equation of Bemis et al., (1998). Following the methods outlined in O'Brien et al. (2017), a value of -1.27‰ VPDB was used for global $\delta^{18}O_{SW.}$ A paleolatitudinal correction was also applied to the global $\delta^{18}O_{SW}$ value (Zachos et al., 1994), using a paleolatitude of 55°S. This approach yields SST estimates of 8–16°C (supplementary information). As with the TEX_{86} values, these data show no discernible stratigraphic trend.

4.1.2 DSDP Site 511

From the TLEs it was possible to quantify GDGT abundances in 79 samples spanning the Cenomanian–Campanian interval. The TEX_{86} values range from 0.53–0.95 (Figure 2); reconstructed paleotemperatures are generally relatively high with values from 17–44.8°C (BAYSPAR; supplementary information). BIT indices range from 0.09 to 0.76, %GDGT-0 from 0 to 96%, Methane Index from 0.18 to 0.88, and ΔRIs from |0.00| to |2.38| (supplementary information). High |ΔRI| values commonly correspond to high BIT, suggesting the influence of terrestrial GDGTs in those samples. After removing samples with unacceptable BIT, %GDGT-0, Methane Index or Ring Index values, 34 samples remained, with TEX_{86} values from 0.69–0.80. These data show a steady decrease in TEX_{86} from the Turonian to the Campanian. There are no trends in the other GDGT indices. T_{max} values were ≤606°C and C_{31}-hopane ratios were 0.22–0.43 (supplementary information).

15 samples contained enough planktic foraminifera for analysis and only 7 of these had enough for multiple analyses of different species. Foraminifera were sparse through large sections of this core, as reported previously (e.g. Huber *et al.,* 1995), which limited sampling. The low abundances of foraminifera (and to some extent also GDGTs) can be attributed to the high clay sedimentation rate through sections of this core (Ludwig *et al.,* 1983). Foraminiferal $\delta^{18}O$ values for these samples range from -3.10 to 0.07 ‰ (Figure 2), corresponding to SSTs of 10–25.5°C. These data show no discernible trend due to the scatter in the values. The $\delta^{13}C$ values exhibit no stratigraphic trend.

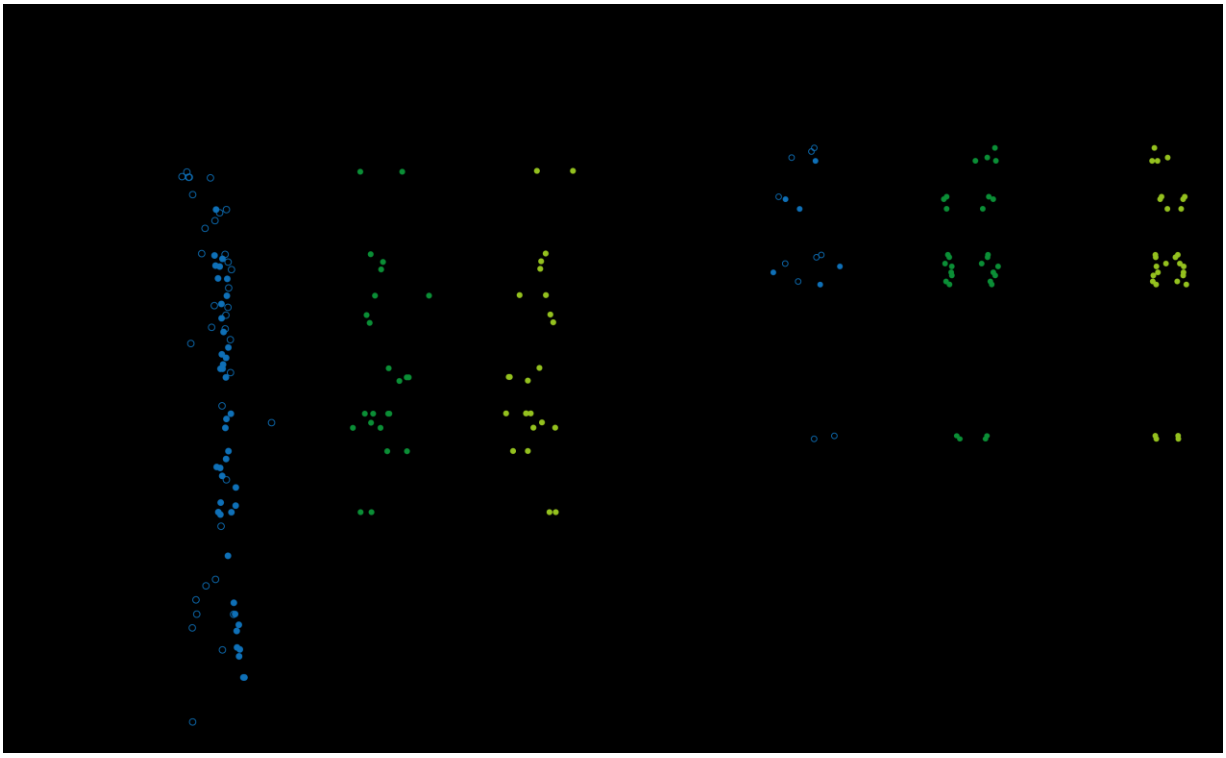

Figure 2. New TEX_{86} and stable-isotope data generated from DSDP Sites 511 and 327, plotted against depth. For TEX_{86} values, closed circles indicate reliable data and open circles indicate samples with GDGT indices exceeding acceptable thresholds (see supplementary information for details).

4.2 Kerguelen Plateau

4.2.1 ODP Site 1135

No GDGTs were detected in the Santonian-Maastrichtian, and in older sediments only 3 samples contained quantifiable GDGTs. These yield TEX_{86} values from 0.74–0.83 (Figure 3), corresponding to SSTs of 29–35.0°C (BAYSPAR; supplementary information). These values are interpreted to reliably reflect SST, as all other GDGT indices have acceptable values (see supplementary information). Only one sample yielded quantifiable C_{31}-hopanes and this sample had a hopane ratio of 0.53 (supplementary information).

Bulk $\delta^{18}O$ values range from -3.56–0.70‰ (Figure 3), increasing steadily from the Cenomanian to the Campanian. $\delta^{13}C_{carb}$ values range from 0.82–3.29‰, showing no stratigraphic trend but two negative excursions at ~308 and 373 m.

4.2.2 ODP Site 1138

15 samples from the Cenomanian and lowest Turonian contained quantifiable GDGTs, yielding TEX_{86} values from 0.83–0.90 (Figure 3), corresponding to SSTs of 27.2–32.8°C (BAYSPAR; supplementary information). These values are interpreted to reliably reflect SSTs, as all other GDGT indices have acceptable values (see supplementary information). TEX_{86} decreases through time.

Bulk carbonate oxygen-isotope values range from -4.73–0.48‰ (Figure 3), increasing steadily from the Turonian to the Maastrichtian. $\delta^{13}C_{carb}$ ranges from 1.32–3.46‰. Negative $\delta^{13}C$

excursions occur at ~640 m, and ~655 m, and positive excursions occur at ~500 , ~630 m, and ~650 m.

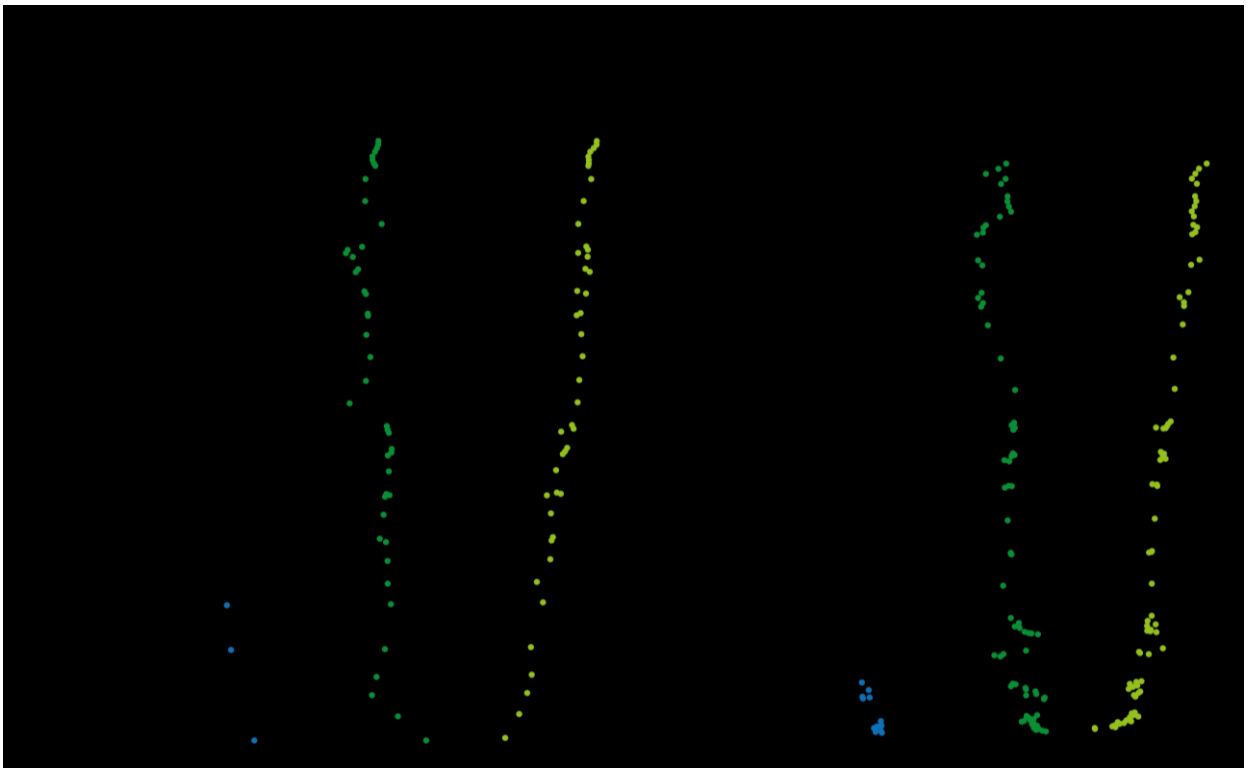

Figure 3. New TEX_{86} and stable-isotope data generated from ODP Sites 1135 and 1138, plotted against depth.

5 Discussion

5.1 TEX_{86} from Falkland Plateau and Kerguelen Plateau

5.1.1 Veracity

A number of samples from Sites 327 and 511 at the Falkland Plateau yielded values for various quality-control indices that suggest their TEX_{86} values might not reflect temperature.

This phenomenon could be due to a range of processes, such as input of terrestrial GDGTs from soils or *in situ* production in the sediments by benthic (methanogenic) archaea. After removing these data points, the remaining TEX_{86} data clearly indicate very high paleotemperatures at these sites during the Late Cretaceous. These data are supported by similar TEX_{86} values from Sites 1135 and 1138 at the Kerguelen Plateau. In isothermal culture studies, the degree of cyclisation decreased with higher rates of ammonia oxidation; higher ammonia oxidation rates (i.e., faster growth rates) produced cooler TEX_{86} temperature estimates, and low ammonia oxidation rates gave warmer temperatures. The authors attribute the correlation between TEX_{86} and temperature to be actually reflecting depth in the water column, which also corresponds with ammonia oxidation. This mechanism is invoked to explain TEX_{86} values indicating warmth in oxygen minimum zones (Basse et al. 2014; Hernández-Sánchez et al. 2014), where ammonia oxidation rates are low, and cold SSTs in high productivity sites such as upwelling zones (Huguet et al. 2007; Lee et al. 2008). Hurley et al. (2016) state that it is possible that the ammonia oxidation rate itself depends on temperature, making the two inseparable variables. However, there is no evidence from the lithology or GDGT ratios to indicate the presence or influence of an oxygen minimum zone on the samples used in this study.

Given the age of these sediments, it is possible that the TEX_{86} values have been altered during burial and thermal degradation. However, with increasing thermal maturity TEX_{86} values generally appear to be biased towards lower SST reconstructions (Schouten et al., 2004). Thermal maturity can be assessed by measuring the abundance of hopanes possessing the biological 17β,21β(H) stereochemical configuration relative to the more thermally stable 17α,21β(H) isomers (Mackenzie et al., 1980). Hopane ratios $(\beta\beta/(\beta\beta+\alpha\beta+\beta\alpha)) < 0.5$ could be associated with sufficiently high thermal maturities that TEX_{86} has been biased (Schouten et al.,

2004). Only one sample from Site 1135 yielded quantifiable C_{31} hopanes, with a ratio of 0.53, indicating thermal maturity too low to impact TEX_{86}. Older, deeper samples from Site 1138 have previously yielded high hopane ratios (~0.5–0.8; Dickson et al., 2017). At both Sites 1135 and 1138, T_{max} values of Upper Cretaceous sediments are low (≤431 °C), supporting the evidence from hopanes for low thermal maturity and no impact on TEX_{86} values.

At Site 511, mid-Jurassic–Upper Cretaceous samples have previously yielded GDGTs and high hopane ratios, suggesting a generally low thermal maturity (Jenkyns et al., 2012). Intriguingly, the samples analyzed in this study from Sites 511 and Site 327 yielded hopane ratios between 0.3 and 0.5, suggesting elevated thermal maturity, which might have influenced TEX_{86}. However, the hopanes are present in very low abundances, and T_{max} values from samples with reliable S2 values (>0.2 mg HC/g TOC; Hart & Steen, 2015; Carvajal-Ortiz & Gentzis, 2015) yield a range of values consistent with both thermal immaturity (< 400 °C) and high maturity (< 463 ˚C). At both sites, the available T_{max} data show no discernible stratigraphic trends.

The conflicting thermal maturity indicators recorded in both Falkland Plateau sites and older sediments at Site 511 (Jenkyns et al., 2012) are difficult to reconcile, suggesting that the maturity recorded by the low-concentrations of organic-matter in the Late Cretaceous sediments may not reflect a primary burial signal, i.e. the hopanes could be associated with reworked kerogen (Handley et al., 2012; Hefter et al., 2017), though previous work suggests no evidence for organic diagenesis (Robert & Malliot, 1983). Irrespective of these different perspectives on the thermal maturity, if *in situ* maturity has affected the TEX_{86} values, then the values measured likely represent minimum estimates of SSTs. As such, thermal diagenesis of the organic matter cannot explain the high temperatures at the Falkland and Kerguelen Plateaus. Therefore, after the

filtering for samples with unreliable index values (i.e. BIT, MI, %GDGT-0, and ΔRI), we consider the remaining TEX_{86} values to be robust indicators of paleotemperature trends.

5.1.2 Temperature trends in TEX_{86}

The similarity of TEX_{86} values during the Turonian at Sites 511 and 1138 and the Santonian at Sites 511 and 1135, suggests that both the Falkland and the Kerguelen Plateau experienced broadly similar long-term trends in SST. Taken together, the data suggest that peak warmth occurred in the early Turonian, followed by a long-term cooling trend into the Santonian and Campanian (Figure 4). This trend is comparable to low- and mid-latitude TEX_{86} records that also show a slow decline in SSTs through to the late Campanian (Forster et al., 2007; Alsenz et al., 2013; Linnert et al., 2014). Around the Cenomanian–Turonian boundary, many sites yield very similar TEX_{86} values, as the proxy is close to the upper limit ($TEX_{86} = 1$) in the low-latitudes (as also noted by Sinninghe Damsté et al., 2010; O'Brien et al., 2017; Robinson et al., 2019). For the upper Turonian to lower Campanian interval, the TEX_{86} data from Sites 511, 1135 and 1138 are offset towards lower values compared with those from lower paleolatitude sites. By contrast, the six TEX_{86} data points from the upper Campanian at Site 327 do not present a consistent pattern. To explore this inconsistency further, it is useful to contextualize these data by comparison with other late Campanian TEX_{86} records. One data point from Site 327 is almost as high as data from Shuqualak, which lies at ~35˚N (Linnert et al., 2014), whereas other samples from Site 327 have TEX_{86} values as low as those from the PAMA Quarry in Israel (0˚ latitude; Alsenz et al., 2013). It has been suggested that the depositional environment at the PAMA Quarry was influenced by upwelling (Alsenz et al., 2013). Such an effect may explain why the PAMA Quarry yields lower TEX_{86} values than Shuqualak (Linnert et al., 2014), that are, perhaps coincidentally the same as those recorded at Site 327. The one sample from Site 327 with a

TEX_{86} value similar to Shuqualak is not easily explained and the limited size of the dataset from Site 327 prohibits a confident interpretation of late Campanian SSTs at the Falkland Plateau.

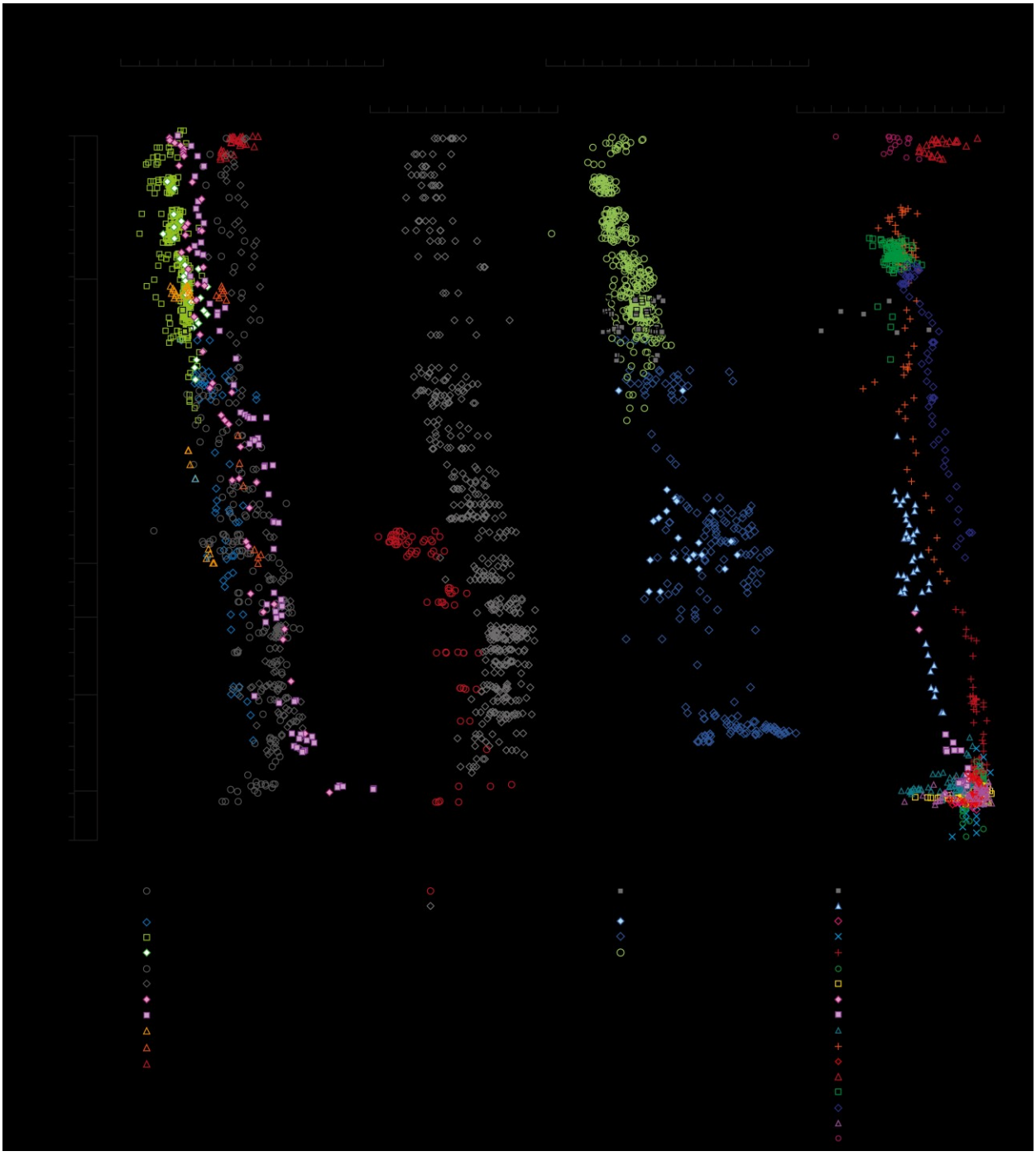

Figure 4. Compilation of benthic foraminiferal $\delta^{18}O$, bulk carbonate $\delta^{18}O$, planktic foraminiferal $\delta^{18}O$, and TEX_{86} data. All oxygen isotope values are reported VPDB. [1]Huber et al., 2018; [2]Huber

et al., 1995; [3]Barrera & Savin, 1999; [4]Friedrich et al., 2009; [5]Barrera & Huber, 1990; [6]Falzoni et al., 2016; [7]Clarke and Jenkyns, 1999; [8]Ando et al., 2013; [9]Woelders et al., 2018; [10]Bice et al., 2003; [11]Forster et al., 2007; [12]Schouten et al., 2003; [13]Bornemann et al., 2008; [14]Sinninghe Damsté et al., 2010; [15]Robinson et al., 2019; [16]Alsenz et al., 2013; [17]van Helmond et al., 2014; [18]Linnert et al., 2014; [19]van Helmond et al., 2015; [20]Woelders et al., 2017. All age models from original sources, plotted on the 2016 timescale. Bulk carbonate and fine-fraction $\delta^{18}O$ values are plotted with the benthic foraminifera $\delta^{18}O$ values as the carbonate is assumed to have either a bottom-water diagenetic overprint and/or offsets related to vital effects in the calcareous nannoplankton that contribute much of carbonate to the sediment (e.g. Falzoni et al., 2016).

5.2 $\delta^{18}O$ values from Falkland Plateau and Kerguelen Plateau

The new Falkland Plateau $\delta^{18}O_{pf}$ data presented here are within the range of previous values (Huber et al., 1995; Barrera & Savin, 1999; Fassell & Bralower, 1999; Bice et al., 2003), albeit with slightly lower maximum temperatures. The most negative $\delta^{18}O_{pf}$ values from Site 511 are as high as those at the Exmouth Plateau, ~10° further north, and the most positive values are comparable to benthic values from sites in both the Atlantic and Tethys (Figure 4). At Site 511, there is an apparent warming event in the Turonian (~91.5 Ma in Figure 4), which has previously been the focus of discussion by Bice et al., (2003). The absence of a similar event in other records (Figure 4) suggests that this might be a consequence of local processes (e.g. local warming, variable preservation and/or species effects). Unfortunately, insufficient GDGTs are preserved in the same interval to test whether SSTs increased locally at that time.

The combined $\delta^{18}O_{pf}$ data from DSDP Sites 327, 511, and 690 (Weddell Sea) show an apparent drastic cooling at ~76 Ma—a trend not seen at other locations. However, this shift

arises largely from a change from samples from the Falkland Plateau to the Weddell Sea, which lies ~10° to the south. The individual sites only show long-term steady cooling.

At Site 1138, bulk-carbonate $\delta^{18}O$ exhibits an apparently sharp increase of about 2‰ in the earliest Turonian following OAE 2, and then a steady increase through to the Campanian (Figure 4). The long-term trend is also observed at Site 1135. The most negative $\delta^{18}O$ at Site 1138 could either be a response to peak warmth in the Early Turonian (e.g. Jenkyns et al., 1994; Robinson et al., 2019) or a consequence of the transition of the seafloor (and hence the diagentic environment) from relatively warm, shallow-water depths in the earliest Turonian to cooler, deeper water environments as the Plateau subsided. This event is not seen in other records (including in the TEX_{86} record from the same site; Robinson et al., 2019) and suggests that it might be predominantly a local environmental signal. However, the gentle increase in $\delta^{18}O$ values from the Turonian to Campanian at Sites 1135 and 1138 shows a strong similarity to planktic foraminiferal, benthic foraminiferal, and bulk carbonate $\delta^{18}O$ values from the Exmouth Plateau, approximately 10˚ further north (Clarke and Jenkyns, 1999; Falzoni et al., 2016) and is thus interpreted to reflect dominantly bottom-water temperature trends. These data further suggest slow, steady cooling through the Late Cretaceous.

5.3 Comparison of trends in $\delta^{18}O$ with TEX_{86}

The overall Late Cretaceous TEX_{86} trend from the Falkland and Kerguelen Plateaus is consistent with the slow, steady cooling inferred from benthic foraminiferal $\delta^{18}O$ and most planktic foraminiferal and bulk carbonate $\delta^{18}O$ records from the South Atlantic and Indian Oceans (Figure 4). However, the evolution of surface-water temperatures through time does show some important differences between both proxies and localities.

For much of the Turonian–mid-Campanian, the benthic compilation, the Indian Ocean planktic foraminiferal $\delta^{18}O$ record from Site 762, and the combined TEX_{86} record from Sites 511, 1135 and 1138 suggests a broadly similar steady trend towards a cooler climate (Figure 4). This trend broadly follows the proxy and model reconstructions of long-term atmospheric CO_2 evolution (e.g. Berner 2006; Foster et al., 2017), which indicate a decrease in its concentration from the mid- to latest Cretaceous. During this same interval, the planktic foraminiferal $\delta^{18}O$ record from Site 511 shows, on average, a similar pattern of cooling but displays considerable scatter and an interval (e.g. ~81 to 78 Ma) in which the lightest $\delta^{18}O$ values are a few per mil greater than those before or after. The scatter in $\delta^{18}O_{pf}$ at Site 511 is largely due to the inclusion here of all planktic species, irrespective of depth habitat. Although the depth habitats of some common taxa have been suggested by cross-plotting carbon and oxygen isotopes, others, most notably *Heterohelix*, exhibit inconsistent behavior (Huber et al., 1995). The apparent cooling in the Campanian (at ~76 Ma) is manifested within the shallow dwelling planktics, which would suggest that this event is not an artifact of changing depth habitats, yet the absence of such an event elsewhere (or in the, albeit limited, TEX_{86} data from Site 511), suggests another explanation is required. One possibility is that the relative paucity of $\delta^{18}O_{pf}$ data through this interval, or subtle differences in carbonate preservation, may be impacting the apparent temperature signal from this site. If this interval is excluded, then the lightest $\delta^{18}O$ values from Site 511 support a broadly smooth cooling trend from the Turonian to the mid-Campanian.

From the mid-Campanian onwards, commonality in trends becomes harder to discern. In the benthic and bulk $\delta^{18}O$ records there is a slight trend towards heavier values, which is also seen in the planktic record from Site 690 in the South Atlantic. In the Indian Ocean at Site 762, planktic $\delta^{18}O$ values appear to show some minor variability over this time. The TEX_{86} records

from the Southern Hemisphere do not, unfortunately, capture this time interval well and the record from Site 327 is, as discussed previously, difficult to interpret. Intriguingly, the planktic foraminifera from Site 327 of late Campanian age suggest cooler conditions on the Falkland Plateau compared to the immediately older samples from Site 511 at ~77 Ma. A similar drop in temperatures is not observed in any other records from the Southern Hemisphere. The range of $\delta^{18}O$ planktic values from Site 327 is less than that from Site 511 and, counter-intuitively, the absolute $\delta^{18}O$ values are as positive as, or more positive than, those observed at Site 690, ~10˚ further south. Surprisingly, our observations indicate that the preservation of the planktic foraminifera from Site 327 is actually better than that at Site 511 (Figure 5), suggesting that diagenesis cannot explain the positive $\delta^{18}O$ values. With all of these uncertainties regarding Site 327, we suggest that the evolution of temperature in the late Campanian was likely not marked by a step-changes in temperature and that for the Falkland Plateau the evolution of temperature from the late Campanian–Maastrichtian remains unresolved.

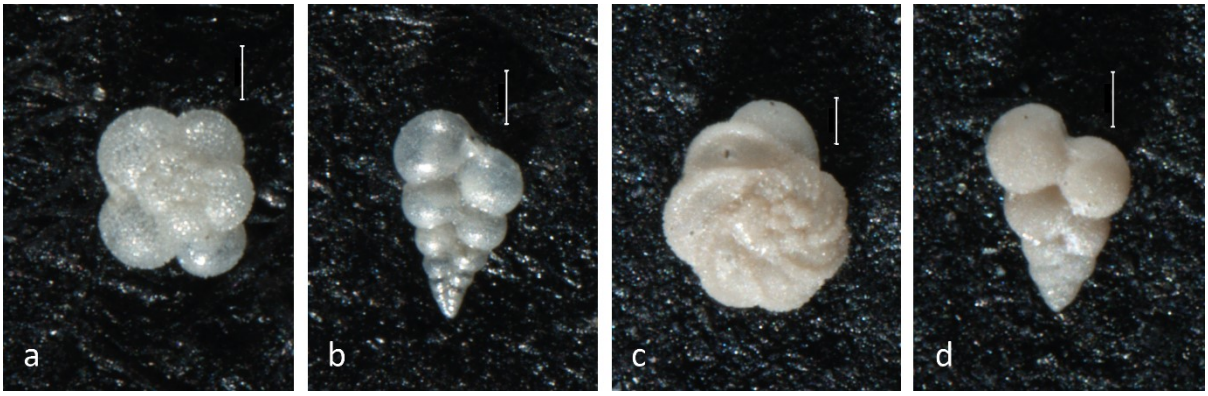

Figure 5. Photographs of planktic foraminifera showing excellent preservation. Scale = 0.1 mm. a) *A. australis* from DSDP Site 327 Core 11 Section 1 50–53 cm; b) *H. planata* from DSDP Site 327 Core 11 Section 1 50–53 cm; c) *M. marginata* from DSDP Site 511 Core 44 Section 5 50–53 cm; d) *H. globulosa* from DSDP Site 511 Core 44 Section 5 50–53 cm .

5.4 Absolute SST value comparison from Site 511 and implications

The absolute values of TEX_{86}-SSTs from the Falkland Plateau (using all three calibrations) are close to the maximum SSTs suggested by planktic foraminiferal $\delta^{18}O$-SST records from the Southern Atlantic and Southern Tethys (e.g. Huber et al., 1995, 2018; Falzoni et al., 2016), and provide further evidence supporting the existence of extremely warm temperatures at southern paleolatitudes of ~55 to 60˚S in the Late Cretaceous (e.g. Huber et al., 1995, 2018; Falzoni et al., 2016). Nonetheless, the SSTs calculated from TEX_{86} at Site 511 are slightly warmer than the corresponding $\delta^{18}O$ values (Figure 6). Unfortunately, only a few samples (n=15) yielded both sufficient GDGTs and planktic foraminifera to directly compare absolute temperatures, but these also indicate that TEX_{86}-derived SSTs are warmer than those derived from $\delta^{18}O$ values. However, such an offset is not unprecedented. In the Cenozoic, TEX_{86} generally agrees well with the trends and absolute temperatures reconstructed from alkenones (e.g. $U^{K'}_{37}$), foraminiferal $\delta^{18}O$ and Mg/Ca ratios, and clumped isotopes (Δ_{47}) of carbonates, though commonly showing a slight offset to warmer SSTs (Zachos et al., 2006; Huguet et al., 2006; Menzel et al., 2006; Pearson et al., 2007; Bijl et al., 2009, 2010; Hollis et al., 2009, 2012; Casteñada et al., 2010; Richey et al., 2010; Keating-Bitonti et al., 2011; Shintani et al., 2011; Lopes dos Santos et al., 2013; Douglas et al., 2014; Meyer et al., 2018; Naafs et al., 2018; Woelders et al., 2018). The causality of these higher temperatures remains unresolved, but has been attributed by many authors to a summer bias of the Thaumarchaeota or a winter bias of the other proxies.

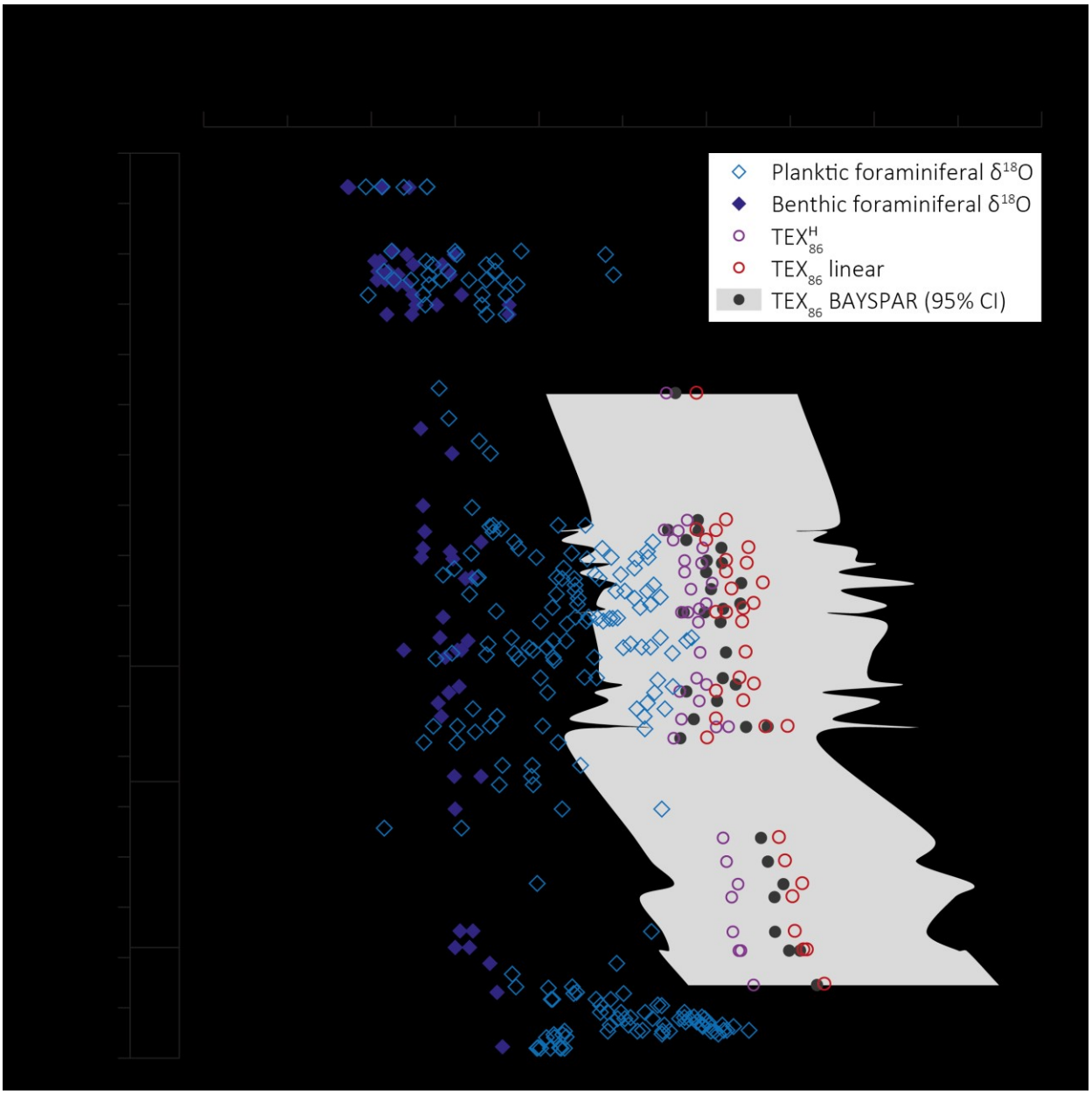

Figure 6. A comparison of benthic and upper ocean temperatures at DSDP Site 511, calculated from $\delta^{18}O$ and TEX_{86}. Planktonic foraminifera include all taxa, irrespective of depth habitat. See 4.1.1. for description of approach used to calculate temperatures from oxygen-isotopes. SSTs were calculated from TEX_{86} using the following empirical calibrations: TEX_{86}^{H} (Kim et al., 2010), TEX_{86}-linear (O'Brien et al., 2017) and the deep-time version of BAYSPAR (Tierney & Tingley, 2014, 2015). Age model from Huber et al. (2018).

TEX_{86} is assumed to reflect mean annual SST, but as nutrient availability, food-web activity, and temperatures vary throughout the year, seasonality in Thaumarchaeotal abundance and export can result in bias. Thaumarchaeota and their GDGTs have been found to exhibit pronounced seasonal variations in the modern ocean, although the timing of peak abundance varies significantly both geographically and environmentally. Observations from sediment traps in the Arabian Sea (Wuchter et al., 2005) and the Mediterranean Sea (Castañeda et al., 2010) indicate a warm (summer) bias in TEX_{86}, whereas data from the North Sea (Wuchter et al., 2005; Pitcher et al., 2011) and Santa Barbara Basin (Huguet et al., 2007) indicate a cold (winter) bias. This effect is exacerbated by the fact that GDGTs almost certainly are produced in the shallow subsurface associated with the zone of maximum ammonia oxidation (Hurley et al., 2018). The strong seasonality in sunlight at high latitudes may further exacerbate any seasonality in nutrient regimes, and thus TEX_{86} in the water column. Nonetheless, despite the indications for highly seasonal GDGT production, sedimentary TEX_{86} values both at a regional (e.g. North Sea; Pitcher et al., 2011) and global scale suggest that the best correlation is obtained between TEX_{86} and mean annual SSTs (Kim et al., 2010).

Foraminiferal tests can undergo alteration via dissolution, recrystallization, and/or the addition of diagenetic calcite overgrowths, all of which have the potential to compromise the $\delta^{18}O$ signal. Calcite precipitated from pore waters during water column, sea-floor and shallow burial recrystallization are generally more enriched in ^{18}O than the original planktonic tests (e.g. Pearson et al., 2001; Pearson 2012), equating to lower paleotemperatures. Despite efforts to select only the best-preserved (glassy) specimens for isotopic analysis, there is a possibility that there is some degree of diagenetic influence on some tests.

Planktic foraminifera can live over a range of depths—from the surface mixed layer to the (sub)thermocline—and therefore over a range of temperatures. The analysis of species from only a certain depth habitat may bias temperature estimates. Foraminifera can change depth habitat over their life cycle; in the modern ocean, many planktic species descend through the water column at maturity to reproduce at greater depths, typically in the upper thermocline (e.g. Hemleben et al., 1989). This behavior can present problems when using foraminiferal $\delta^{18}O$ for SST reconstructions as the descent through the water column can bias temperature estimates to the colder values at depth. Ontogeny can also bias $\delta^{18}O$ values, as the metabolic rates of foraminifera were found to change throughout their life cycle (Spero & Lea, 1996), with decreasing ^{18}O depletion with age. If fractionation and depth habitat change with age, the $\delta^{18}O$ signal can be offset from SST. As such, this ontongenic effect can skew temperature estimates towards the more abundant size fraction/age.

While there are many caveats to the use of both TEX_{86} and foraminiferal $\delta^{18}O$, with appropriate screening both are valuable tools for paleoclimate reconstruction. However, the contrast in reconstructed temperatures and trends at Site 511 suggests that (at least) one of the proxies at this location does not record mean annual SST. The Site 511 TEX_{86} values also exhibit a strong similarity to the Site 511 benthic record as well as the global compilation of TEX_{86}, planktic $\delta^{18}O$, and benthic $\delta^{18}O$ records, suggesting that the TEX_{86} record accurately reflects long-term regional and global climatic trends. As noted previously, although isoprenoid GDGTs are produced throughout the water column (Shah et al., 2008), modern sedimentary TEX_{86} values correlate best with SSTs suggesting that the dominant signal in sediments is exported from the surface ocean (e.g. Schouten et al., 2013). Thus the similarity in trends at Site 511 between benthic temperatures and TEX_{86} reflects temperature throughout the water column. In contrast to

the TEX_{86} and benthic records, the planktic $\delta^{18}O$ values show much more temporal variability, likely reflecting short-term changes in climate and environment, and/or the effects of subtle diagenesis and under sampling.

In general, all proxy data indicate very high SSTs in the southern mid/high latitudes during the Late Cretaceous. If correct, then why do models struggle to reproduce such warmth and reduced latitudinal gradients? A long-standing problem in paleoclimatology is the discrepancy between proxy data and model simulations for high latitudes in a greenhouse world. Proxy records indicate equable conditions and reduced latitudinal temperature gradients (e.g. Huber et al. 1995; Huber et al. 2002; Amiot et al. 2004; Pearson et al. 2007; Hollis et al. 2009; Sinninghe Damsté et al. 2010; Keating-Bitonti et al. 2011; Naafs et al., 2018), whereas models indicate cooler polar conditions and steeper latitudinal gradients (Barron 1987; Huber & Sloan 1999, 2001; Bice et al. 2006; Huber & Caballero 2011; Lunt et al. 2012; Upchurch et al. 2015; Lunt et al. 2016; Tabor et al. 2016).

Warming appears to be amplified in the polar regions, particularly in periods of extreme warmth (Huber et al. 2000; Johannessen et al. 2004; Sluijs et al. 2006; Miller et al. 2010; Lee 2014), leading to reduced latitudinal temperature gradients. Climate modelling demonstrates that the contributions to polar amplification include the greenhouse effect of CO_2 (Manabe & Wetherald 1980), additional water vapor (Graversen & Wang 2009), cloud feedbacks (Sloan & Pollard 1998; Vavrus 2004; Kump & Pollard 2008; Kiehl & Shields, 2013; Sagoo et al., 2013), methane concentration (Kirk-Davidoff et al. 2002; Schmidt & Shindell 2003; Bice et al. 2006), vegetation–climate interactions (Zhou et al. 2012), and/or changes in atmospheric (Manabe & Wetherald 1980) and oceanic heat transport (Holland & Bitz 2003; Khodri et al. 2001; Spielhagen et al. 2001). One study found that at high temperatures the greatest contribution to

polar amplification derives from temperature feedbacks wherein more energy is radiated back into space from the tropics than the poles (Pithan & Mauritsen 2014). However, the relative influence of these drivers is debated, and these studies suggest that no single mechanism can produce the temperatures and latitudinal gradients such as those suggested for the Cretaceous and early Paleogene, but rather a complex interplay of multiple drivers is required. For example, through the addition of CH_4 and stratospheric water vapor, Schmidt & Shindell (2003) were able to reconcile global warmth of the PETM without a significant CO_2 increase. Other studies maintain that methane production must be consistently high for stratospheric water vapor to drive warming (Sloan & Pollard 1998; Kirk-Davidoff et al. 2002).

It appears that previous models of greenhouse climate lack the physio-chemical inputs that allow for the magnitude of polar amplification recorded by a range of temperature proxies. With sufficiently high CO_2, models are increasingly showing agreement with proxy records, especially terrestrial data (e.g. Huber et al., 2011; Lunt et al. 2012), but the mechanisms vary between different models. Comparisons with SST data are also improving, though problems remain with high latitudes; for example, $\delta^{18}O$- and TEX_{86}-SST uncertainties only just overlap with that of the model for the Eocene (Lunt et al. 2012). However, if seasonality is an important component of some Late Cretaceous proxy reconstructions then this could lead to discrepancies in model-data comparisons that cannot be easily accounted for without better approaches to determining the seasonal influence on planktic organisms in the geological record.

6. Conclusions

New TEX_{86}- and $\delta^{18}O$-SST estimates from the Falkland Plateau confirm previous studies indicating extreme warmth through the Late Cretaceous at the high southern latitudes, suggesting

that the depleted $\delta^{18}O$ values cannot simply be ascribed to diagenesis or anomalously light $\delta^{18}O_{SW}$. The compilation of data from the Falkland and Kerguelen Plateaus indicates high SSTs across the southern high-latitudes, and steady cooling from the Turonian to Campanian. The extreme warmth in the southern high latitudes suggests that latitudinal gradients remained low throughout the Late Cretaceous, and that polar ice caps at low altitudes are hence deemed unlikely.

Because both the TEX_{86} and $\delta^{18}O_{pf}$ data from Site 327 on the Falkland Plateau are interpreted to be problematic and are therefore excluded at this point, it is suggested that the evolution of temperature in the late Campanian was likely not marked by any step-changes in temperature and that, for the Falkland Plateau, the exact pattern of climate change from the late Campanian–Maastrichtian remains unresolved. However, with so little data, and from so few sites, it is difficult to determine precise climate dynamics in the Late Cretaceous southern high-latitudes, impeding the accurate modelling of global climate at this time.

When compared to other data from a similar paleolatitude, it appears that the Falkland Plateau SSTs are not especially anomalous, indicating a global forcing mechanism, probably a combination of elevated atmospheric CO_2, CH_4, and water vapor. However, the precise tectonic and volcanic mechanisms by which CO_2 remained high, the sources and amount of atmospheric methane, and the role of the hydrological cycle in greenhouse climates, remain issues that, although debated over decades, are still to be fully resolved. This problem highlights the fact that major uncertainties exist in our understanding of Late Cretaceous carbon cycling and climate and the operation of the Earth system in a greenhouse world.

Acknowledgments, Samples, and Data

We thank Charlotte O'Brien for calculating the BAYSPAR TEX_{86} values, Brian Huber for his help in the identification of foraminifera, and the IODP for access to samples. L.K.O. would like to thank the Clarendon Fund (University of Oxford) and University College, Oxford, for supporting her DPhil. S.A.R. and R.D.P. acknowledge the receipt of support from the Natural Environment Research Council (NERC, UK; NE/K014757/1, NE/K012479/1). B.D.A.N. is funded through a Royal Society Tata University Research Fellowship and R.D.P. acknowledges the Royal Society Wolfson Research Merit Award. We thank the reviewers for their useful comments. Data are available in the supplement.

References

Alsenz, H., Regnery, J., Ashckenazi-Polivoda, S., Meilijson, A., Ron-Yankovich, L., Abramovich, S., et al. (2013). Sea surface temperature record of a Late Cretaceous tropical southern Tethys upwelling system. *Palaeogeography, Palaeoclimatology, Palaeoecology*, *392*, 350–358. doi:10.1016/j.palaeo.2013.09.013

Amiot, R., Lécuyer, C., Buffetaut, E., Fluteau, F., Legendre, S., & Martineau, F. (2004). Latitudinal temperature gradient during the Cretaceous Upper Campanian–Middle Maastrichtian: $\delta^{18}O$ record of continental vertebrates. *Earth and Planetary Science Letters*, 226, 255–272. doi:10.1016/j.epsl.2004.07.015

Ando, A., Woodard, S. C., Evans, H. F., Littler, K., Herrmann, S., Macleod, K. G., et al. (2013). An emerging palaeoceanographic "missing link": multidisciplinary study of rarely

recovered parts of deep-sea Santonian–Campanian transition from Shatsky Rise. *Journal of the Geological Society, 170*(3), 381–384. doi:10.1144/jgs2012-137

Barker, P. F., Dalziel, I. W. D., & Wise, S. W. (1977b). Introduction. *In* Barker, P. F., Dalziel, I.W.D. et al., *Initial Reports of the Deep Sea Drilling Project*, 36: Washington (U.S. Government Printing Office). doi:10.2973/dsdp.proc.36.101.1977

Barker, P. F., Dalziel, I. W. D., Dinkelman, M. G., Elliot, D. H., Gombos, A. M., Jr., Lonardi, A., et al. (1977a). Site 328. *In* Barker, P. F., Dalziel, I.W.D. et al., *Initial Reports of the Deep Sea Drilling Project*, 36: Washington (U.S. Government Printing Office). doi:10.2973/dsdp.proc.36.104.1977

Barker, P. F., Dalziel, I. W. D., Dinkelman, M. G., Elliot, D. H., Gombos, A. M., Jr., Lonardi, A., et al. (1977c). Site 327. *In* Barker, P. F., Dalziel, I.W.D. et al., *Initial Reports of the Deep Sea Drilling Project*, 36: Washington (U.S. Government Printing Office). doi:10.2973/dsdp.proc.36.103.1977

Barrera, E., & Huber, B. T. (1990). Evolution of Antarctic Waters during the Maestrichtian: Foraminifer Oxygen and Carbon Isotope Ratios, Leg 113. *Proceedings of the Ocean Drilling Program.* doi:10.2973/odp.proc.sr.113.137.1990

Barrera, E., & Savin, S. M. (1999). Evolution of late Campanian-Maastrichtian marine climates and oceans. *GSA Special Paper 332: Evolution of the Cretaceous Ocean-Climate System*, 245–282. doi:10.1130/0-8137-2332-9.245

Barron, E.J. (1987). Cretaceous plate tectonic reconstructions. *Palaeogeography, Palaeoclimatology, Palaeoecology*, *59*, 3–29. doi:10.1016/0031-0182(87)90071-x

Behar, F., Beaumont, V., & De B. Penteado, H. L. (2001). Rock-Eval 6 Technology:

Performances and Developments. *Oil & Gas Science and Technology, 56*(2), 111–134. doi:10.2516/ogst:2001013

Basse, A., Zhu, C., Versteegh, G. J. M., Fischer, G., Hinrichs, K.-U., & Mollenhauer, G. (2014). Distribution of intact and core tetraether lipids in water column profiles of suspended particulate matter off Cape Blanc, NW Africa. *Organic Geochemistry*, 72, 1–13. doi:10.1016/j.orggeochem.2014.04.007

Bemis, B. E., Spero, H. J., Bijma, J., & Lea, D. W. (1998). Reevaluation of the oxygen isotopic composition of planktonic foraminifera: Experimental results and revised paleotemperature equations. *Paleoceanography*, 13(2), 150–160. doi:10.1029/98pa00070

Berner, R. A. (2006). GEOCARBSULF: A combined model for Phanerozoic atmospheric O2 and CO_2. *Geochimica et Cosmochimica Acta*, 70(23), 5653–5664. doi:10.1016/j.gca.2005.11.032.

Bice, K. L., Birgel, D., Meyers, P. A., Dahl, K. A., Hinrichs, K.-U., & Norris, R. D. (2006). A multiple proxy and model study of Cretaceous upper ocean temperatures and atmospheric CO_2 concentrations. *Paleoceanography*, 21(2). doi:10.1029/2005pa001203

Bice, K. L., Huber, B. T., & Norris, R. D. (2003). Extreme polar warmth during the Cretaceous greenhouse? Paradox of the late Turonian $\delta^{18}O$ record at Deep Sea Drilling Project Site 511. *Paleoceanography*, 18(2). doi:10.1029/2002pa000848

Bijl, P. K., Houben, A. J. P., Schouten, S., Bohaty, S. M., Sluijs, A., Reichart, G.-J., et al. (2010). Transient Middle Eocene Atmospheric CO_2 and Temperature Variations. *Science*, 330(6005), 819–821. doi:10.1126/science.1193654

Bijl, P. K., Schouten, S., Sluijs, A., Reichart, G.-J., Zachos, J. C., & Brinkhuis, H. (2009).

Early Palaeogene temperature evolution of the southwest Pacific Ocean. *Nature*, 461(7265), 776–779. doi:10.1038/nature08399

Blakey, R., 2016. Global Paleogeography, <www2.nau.edu/rcb7/globaltext2.html>.

Bornemann, A., Norris, R. D., Friedrich, O., Beckmann, B., Schouten, S., Damste, J. S. S., et al. (2008). Isotopic Evidence for Glaciation During the Cretaceous Supergreenhouse. *Science*, 319(5860), 189–192. doi:10.1126/science.1148777

Bowman, V. C., Francis, J. E., & Riding, J. B. (2013). Late Cretaceous winter sea ice in Antarctica? *Geology*, 41(12), 1227–1230. doi:10.1130/g34891.1

Carvajal-Ortiz, H., & Gentzis, T. (2015). Critical considerations when assessing hydrocarbon plays using Rock-Eval pyrolysis and organic petrology data: Data quality revisited. *International Journal of Coal Geology*, 152, 113–122. doi:10.1016/j.coal.2015.06.001

Castañeda, I. S., Schefuß, E., Pätzold, J., Sinninghe Damsté, J. S., Weldeab, S., & Schouten, S. (2010). Millennial-scale sea surface temperature changes in the eastern Mediterranean (Nile River Delta region) over the last 27,000 years. *Paleoceanography*, 25(1). doi:10.1029/2009pa001740

Clarke, L.J. & Jenkyns, H.C., 1999. New oxygen isotope evidence for long-term Cretaceous climatic change in the Southern Hemisphere. *Geology*, 27 (8): 699–702. doi:10.1130/0091-7613(1999)027<0699:NOIEFL>2.3.CO;2

Coffin, M. F., Frey, F. A., & Wallace, P. J. (Eds). (2000). Proceedings of the Ocean Drilling Program, 183 Initial Reports. *Proceedings of the Ocean Drilling Program*. doi:10.2973/odp.proc.ir.183.2000

Davies, A., Kemp, A. E. S., & Pike, J. (2009). Late Cretaceous seasonal ocean variability

from the Arctic. *Nature*, 460(7252), 254–258. doi:10.1038/nature08141

Dickson, A. J., Saker-Clark, M., Jenkyns, H. C., Bottini, C., Erba, E., Russo, F., et al. (2017). A Southern Hemisphere record of global trace-metal drawdown and orbital modulation of organic-matter burial across the Cenomanian-Turonian boundary (Ocean Drilling Program Site 1138, Kerguelen Plateau). *Sedimentology*, 64(1), 186–203. doi:10.1111/sed.12303

Duplessy, J. C., Bé, A. W. H., & Blanc, P. L. (1981). Oxygen and carbon isotopic composition and biogeographic distribution of planktonic foraminifera in the Indian Ocean. *Palaeogeography, Palaeoclimatology, Palaeoecology*, 33(1–3), 9–46. doi:10.1016/0031-0182(81)90031-6

Falzoni, F., Petrizzo, M. R., Clarke, L. J., MacLeod, K. G., & Jenkyns, H. C. (2016). Long-term Late Cretaceous oxygen- and carbon-isotope trends and planktonic foraminiferal turnover: A new record from the southern midlatitudes. *Geological Society of America Bulletin*, 128(11–12), 1725–1735. doi:10.1130/b31399.1

Fassell, M. L., & Bralower, T. J. (1999). Warm, equable Mid-Cretaceous: Stable isotope evidence. *GSA Special Paper 332: Evolution of the Cretaceous Ocean-Climate System,* 121–142. doi:10.1130/0-8137-2332-9.121

Forster, A., Schouten, S., Baas, M., & Sinninghe Damsté, J. S. (2007). Mid-Cretaceous (Albian–Santonian) sea surface temperature record of the tropical Atlantic Ocean. *Geology*, 35(10), 919. doi:10.1130/g23874a.1

Foster, G. L., Royer, D. L., & Lunt, D. J. (2017). Future climate forcing potentially without precedent in the last 420 million years. *Nature Communications*, 8, 14845. doi:10.1038/ncomms14845

Frey, F. A., Coffin, M. F., Wallace, P. J., Weis, D., Zhao, X., Wise, S. W., … Antretter, M. (2000). Origin and evolution of a submarine large igneous province: the Kerguelen Plateau and Broken Ridge, southern Indian Ocean. *Earth and Planetary Science Letters*, 176(1), 73–89. doi:10.1016/s0012-821x(99)00315-5

Friedrich, O., Herrle, J. O., Wilson, P. A., Cooper, M. J., Erbacher, J., & Hemleben, C. (2009). Early Maastrichtian carbon cycle perturbation and cooling event: Implications from the South Atlantic Ocean. *Paleoceanography, 24*(2). doi:10.1029/2008pa001654

Friedrich, O., Norris, R. D., & Erbacher, J. (2012). Evolution of middle to Late Cretaceous oceans—a 55 my record of Earth's temperature and carbon cycle. *Geology*, 40(2), 107–110. doi: https://doi:10.1130/G32701.1

Gale, A. S., Hardenbol, J., Hathway, B., Kennedy, W. J., Young, J. R., & Phansalkar, V. (2002). Global correlation of Cenomanian (Upper Cretaceous) sequences: Evidence for Milankovitch control on sea level. *Geology*, *30*(4), 291–294. doi: https://doi:10.1130/0091-7613(2002)030<0291:GCOCUC>2.0.CO;2

Galeotti, S., Rusciadelli, G., Sprovieri, M., Lanci, L., Gaudio, A., & Pekar, S. (2009). Sea-level control on facies architecture in the Cenomanian–Coniacian Apulian margin (Western Tethys): A record of glacio-eustatic fluctuations during the Cretaceous greenhouse? *Palaeogeography, Palaeoclimatology, Palaeoecology*, 276(1–4), 196–205. doi:10.1016/j.palaeo.2009.03.011

Graversen, R. G., & Wang, M. (2009). Polar amplification in a coupled climate model with locked albedo. *Climate Dynamics*, 33(5), 629–643. doi:10.1007/s00382-009-0535-6

Handley, L., O'Halloran, A., Pearson, P. N., Hawkins, E., Nicholas, C. J., Schouten, S., et

al. (2012). Changes in the hydrological cycle in tropical East Africa during the Paleocene–Eocene Thermal Maximum. *Palaeogeography, Palaeoclimatology, Palaeoecology*, 329–330, 10–21. doi:10.1016/j.palaeo.2012.02.002

Hart, B. S., & Steen, A. S. (2015). Programmed pyrolysis (Rock-Eval) data and shale paleoenvironmental analyses: A review. *Interpretation*, 3(1), SH41–SH58. doi:10.1190/int-2014-0168.1

Hay, W. W., DeConto, R. M., Wold, C. N., Wilson, K. M., Voigt, S., Schulz, M., … Söding, E. (1999). Alternative global Cretaceous paleogeography. *GSA Special Paper 332: Evolution of the Cretaceous Ocean-Climate System*, 1–47. doi:10.1130/0-8137-2332-9.1

Hefter, J., Naafs, B. D. A., & Zhang, S. (2017). Tracing the source of ancient reworked organic matter delivered to the North Atlantic Ocean during Heinrich Events. *Geochimica et Cosmochimica Acta*, 205, 211–225. doi:10.1016/j.gca.2017.02.008

Hemleben, C., Spindler, M., & Anderson, O. R. (1989). *Modern Planktonic Foraminifera*. xiii+ 363 pp. New York, Berlin, Heidelberg, London, Paris, Tokyo: Springer-Verlag. Price DM 178.00 (hard covers) ISBN 3 540 96815 6. *Geological Magazine*, *126*(6), 735–736. doi:10.1007/978-1-4612-3544-6

Hernández-Sánchez, M. T., Woodward, E. M. S., Taylor, K. W. R., Henderson, G. M., & Pancost, R. D. (2014). Variations in GDGT distributions through the water column in the South East Atlantic Ocean. *Geochimica et Cosmochimica Acta*, 132, 337-348. doi:10.1016/j.gca.2014.02.009

Holland, M. M., & Bitz, C. M. (2003). Polar amplification of climate change in coupled models. *Climate Dynamics*, 21(3–4), 221–232. doi:10.1007/s00382-003-0332-6

Hollis, C. J., Handley, L., Crouch, E. M., Morgans, H. E. G., Baker, J. A., Creech, J., et al. (2009). Tropical sea temperatures in the high-latitude South Pacific during the Eocene. *Geology*, 37(2), 99–102. doi:10.1130/g25200a.1

Hollis, C. J., Taylor, K. W. R., Handley, L., Pancost, R. D., Huber, M., Creech, J. B., et al. (2012). Early Paleogene temperature history of the Southwest Pacific Ocean: Reconciling proxies and models. *Earth and Planetary Science Letters*, 349–350, 53–66. doi:10.1016/j.epsl.2012.06.024

Hopmans, E. C., Schouten, S., & Sinninghe Damsté, J. S. (2016). The effect of improved chromatography on GDGT-based palaeoproxies. *Organic Geochemistry*, 93, 1–6. doi:10.1016/j.orggeochem.2015.12.006

Hopmans, E. C., Weijers, J. W. ., Schefuß, E., Herfort, L., Sinninghe Damsté, J. S., & Schouten, S. (2004). A novel proxy for terrestrial organic matter in sediments based on branched and isoprenoid tetraether lipids. *Earth and Planetary Science Letters*, 224(1–2), 107–116. doi:10.1016/j.epsl.2004.05.012

Huber, B. T., Hodell, D. A., & Hamilton, C. P. (1995). Middle–Late Cretaceous climate of the southern high latitudes: stable isotopic evidence for minimal equator-to-pole thermal gradients. *Geological Society of America Bulletin*, 107(10), 1164–1191. doi: https://doi:10.1130/0016-7606(1995)107<1164:MLCCOT>2.3.CO;2

Huber, B. T., MacLeod, K. G., Watkins, D. K., & Coffin, M. F. (2018). The rise and fall of the Cretaceous Hot Greenhouse climate. *Global and Planetary Change*, 167, 1–23. doi:10.1016/j.gloplacha.2018.04.004

Huber, B. T., Norris, R. D., & MacLeod, K. G. (2002). Deep-sea paleotemperature record of

extreme warmth during the Cretaceous. *Geology*, 30(2), 123–126. doi: https://doi:10.1130/0091-7613(2002)030<0123:DSPROE>2.0.CO;2

Huber, M., & Caballero, R. (2011). The early Eocene equable climate problem revisited. *Climate of the Past*, 7(2), 603–633. doi:10.5194/cp-7-603-2011

Huber, M., & Sloan, L. C. (1999). Warm climate transitions: A general circulation modeling study of the Late Paleocene Thermal Maximum (~56 Ma). *Journal of Geophysical Research: Atmospheres*, 104, D14, 16633–16655. doi:10.1029/1999jd900272

Huber, M., & Sloan, L. C. (2001). Heat transport, deep waters, and thermal gradients: Coupled simulation of an Eocene greenhouse climate. *Geophysical Research Letters*, 28(18), 3481–3484. doi:10.1029/2001gl012943

Huguet, C., Hopmans, E. C., Febo-Ayala, W., Thompson, D. H., Sinninghe Damsté, J. S., & Schouten, S. (2006). An improved method to determine the absolute abundance of glycerol dibiphytanyl glycerol tetraether lipids. *Organic Geochemistry*, 37(9), 1036–1041. doi:10.1016/j.orggeochem.2006.05.008

Huguet, C., Schimmelmann, A., Thunell, R., Lourens, L. J., Sinninghe Damsté, J. S., & Schouten, S. (2007). A study of the TEX_{86} paleothermometer in the water column and sediments of the Santa Barbara Basin, California. *Paleoceanography*, 22(3). doi:10.1029/2006pa001310

Hurley, S. J., Elling, F. J., Könneke, M., Buchwald, C., Wankel, S. D., Santoro, A. E., et al. (2016). Influence of ammonia oxidation rate on thaumarchaeal lipid composition and the TEX_{86} temperature proxy. *Proceedings of the National Academy of Sciences*, 113(28), 7762–7767. doi:10.1073/pnas.1518534113

Hurley, S. J., Lipp, J. S., Close, H. G., Hinrichs, K.-U., & Pearson, A. (2018). Distribution

and export of isoprenoid tetraether lipids in suspended particulate matter from the water column of the Western Atlantic Ocean. *Organic Geochemistry*, 116, 90–102. doi:10.1016/j.orggeochem.2017.11.010

Jenkyns, H. C., Gale, A. S., & Corfield, R. M. (1994). Carbon- and oxygen-isotope stratigraphy of the English Chalk and Italian Scaglia and its palaeoclimatic significance. *Geological Magazine, 131*(01), 1–34. doi:10.1017/s0016756800010451

Jenkyns, H. C., Schouten-Huibers, L., Schouten, S., & Sinninghe Damsté, J. S. (2012). Warm Middle Jurassic–Early Cretaceous high-latitude sea-surface temperatures from the Southern Ocean. *Climate of the Past*, 8(1), 215–226. doi:10.5194/cp-8-215-2012

Johannessen, O. M., Bengtsson, L., Miles, M. W., Kuzmina, S. I., Semenov, V. A., Alekseev, G. V., et al. (2004). Arctic climate change: observed and modelled temperature and sea-ice variability. *Tellus A*, 56(4), 328–341. doi:10.1111/j.1600-0870.2004.00060.x

Keating-Bitonti, C. R., Ivany, L. C., Affek, H. P., Douglas, P., & Samson, S. D. (2011). Warm, not super-hot, temperatures in the early Eocene subtropics. *Geology*, 39(8), 771–774. doi:10.1130/g32054.1

Khodri, M., Leclainche, Y., Ramstein, G., Braconnot, P., Marti, O., & Cortijo, E. (2001). Simulating the amplification of orbital forcing by ocean feedbacks in the last glaciation. *Nature*, 410(6828), 570–574. doi:10.1038/35069044

Kiehl, J.T., Shields, C.A. (2013). Sensitivity of the Palaeocene–Eocene Thermal Maximum climate to cloud properties. *Philosophical Transactions of the Royal Society of London A: Mathematical, Physical and Engineering Sciences*, 371(2001), doi: 10.1098/rsta.2013.0093

Kim, J.-H., Schouten, S., Hopmans, E. C., Donner, B., & Sinninghe Damsté, J. S. (2008).

Global sediment core-top calibration of the TEX_{86} paleothermometer in the ocean. *Geochimica et Cosmochimica Acta*, 72(4), 1154–1173. doi:10.1016/j.gca.2007.12.010

Kim, J.-H., van der Meer, J., Schouten, S., Helmke, P., Willmott, V., Sangiorgi, F., Koç, N., Hopmans, E.C., Sinninghe Damsté, J.S., 2010. New indices and calibrations derived from the distribution of crenarchaeal isoprenoid tetraether lipids: Implications for past sea surface temperature reconstructions. *Geochimica et Cosmochimica Acta*, 74, 4639–4654, doi: 10.1016/j.gca.2010.05.027

Kirk-Davidoff, D. B. (2002). On the feedback of stratospheric clouds on polar climate. *Geophysical Research Letters*, 29(11). doi:10.1029/2002gl014659

Krasheninnikov, V. A., & Basov, I. A. (1983). Stratigraphy of Cretaceous Sediments of the Falkland Plateau Based on Planktonic Foraminifers, Deep Sea Drilling Project Leg 71. *In* Ludwig, W. J., Krasheninikov, V. A., et al., *Initial Reports of the Deep Sea Drilling Project,* 71: Washington (U.S. Govt. Printing Office). doi:10.2973/dsdp.proc.71.129.1983

Kump, L. R., & Pollard, D. (2008). Amplification of Cretaceous Warmth by Biological Cloud Feedbacks. *Science*, 320(5873), 195–195. doi:10.1126/science.1153883

Lee, S. (2014). A theory for polar amplification from a general circulation perspective. *Asia-Pacific Journal of Atmospheric Sciences*, 50(1), 31–43. doi:10.1007/s13143-014-0024-7

Lee, K. E., Kim, J.-H., Wilke, I., Helmke, P., & Schouten, S. (2008). A study of the alkenone, TEX_{86}, and planktonic foraminifera in the Benguela Upwelling System: Implications for past sea surface temperature estimates. *Geochemistry, Geophysics, Geosystems*, 9(10). doi:10.1029/2008gc002056

Li, L., Keller, G., Adatte, T., & Stinnesbeck, W. (2000). Late Cretaceous sea-level changes

in Tunisia: a multi-disciplinary approach. *Journal of the Geological Society*, 157(2), 447–458. doi:10.1144/jgs.157.2.447

Linnert, C., Robinson, S. A., Lees, J. A., Bown, P. R., Pérez-Rodríguez, I., Petrizzo, M. R., et al. (2014). Evidence for global cooling in the Late Cretaceous. *Nature Communications*, 5(1). doi:10.1038/ncomms5194

Littler, K., Robinson, S. A., Bown, P. R., Nederbragt, A. J., & Pancost, R. D. (2011). High sea-surface temperatures during the Early Cretaceous Epoch. *Nature Geoscience*, 4(3), 169–172. doi:10.1038/ngeo1081

Lopes dos Santos, R.A., Spooner, M. I., Barrows, T. T., De Deckker, P., Damste, J. S. S., & Schouten, S., 2013. Comparison of organic ($U^{K'}_{37}$, TEX^{H}_{86}, LDI) and faunal proxies (foraminiferal assemblages) for reconstruction of late Quaternary sea surface temperature variability from offshore southeastern Australia. *Paleoceanography*, *28*(3), 377–387. doi:10.1002/palo.20035

Ludwig, W. J., Krasheninnikov, V. A., & Wise, S. W. (1983). Introduction and Explanatory Notes. *In* Ludwig, W. J., Krasheninikov, V. A., et al., *Initial Reports of the Deep Sea Drilling Project,* 71: Washington (U.S. Govt. Printing Office). doi:10.2973/dsdp.proc.71.101.1983

Lunt, D. J., Dunkley Jones, T., Heinemann, M., Huber, M., LeGrande, A., Winguth, A., et al. (2012). A model–data comparison for a multi-model ensemble of early Eocene atmosphere–ocean simulations: EoMIP. *Climate of the Past*, 8(5), 1717–1736. doi:10.5194/cp-8-1717-2012

Lunt, D. J., Farnsworth, A., Loptson, C., Foster, G. L., Markwick, P., O'Brien, C. L., … Wrobel, N. (2015). Palaeogeographic controls on climate and proxy interpretation. *Climate of the Past Discussions*, 11(6), 5683–5725. doi:10.5194/cpd-11-5683-2015

Mackenzie, A. S., Patience, R. L., Maxwell, J. R., Vandenbroucke, M., & Durand, B. (1980).

Molecular parameters of maturation in the Toarcian shales, Paris Basin, France—I. Changes in the configurations of acyclic isoprenoid alkanes, steranes and triterpanes. *Geochimica et Cosmochimica Acta*, 44(11), 1709–1721. doi:10.1016/0016-7037(80)90222-7

MacLeod, K. G., Huber, B. T., & Isaza-Londoño, C. (2005). North Atlantic warming during global cooling at the end of the Cretaceous. *Geology*, 33(6), 437. doi:10.1130/g21466.1

MacLeod, K. G., Huber, B. T., Berrocoso, Á. J., & Wendler, I. (2013). A stable and hot Turonian without glacial $\delta^{18}O$ excursions is indicated by exquisitely preserved Tanzanian foraminifera. *Geology*, 41(10), 1083–1086. doi:10.1130/g34510.1

Manabe, S., & Wetherald, R. T. (1980). On the distribution of climate change resulting from an increase in CO2 content of the atmosphere. *Journal of the Atmospheric Sciences*, *37*(1), 99–118. doi: 10.1175/1520-0469(1980)037<0099:OTDOCC>2.0.CO;2

Menzel, D., Hopmans, E. C., Schouten, S., & Sinninghe Damsté, J. S. (2006). Membrane tetraether lipids of planktonic Crenarchaeota in Pliocene sapropels of the eastern Mediterranean Sea. *Palaeogeography, Palaeoclimatology, Palaeoecology*, 239(1–2), 1–15. doi:10.1016/j.palaeo.2006.01.002

Meyers, P. A., Yum, J.-G., & Wise, S. W. (2009). Origins and maturity of organic matter in mid-Cretaceous black shales from ODP Site 1138 on the Kerguelen Plateau. Marine and Petroleum *Geology*, 26(6), 909–915. doi:10.1016/j.marpetgeo.2008.09.003

Mohr, B. A. R., Wähnert, V., & Lazarus, D. (2002). Mid-Cretaceous Paleobotany and Palynology of the Central Kerguelen Plateau, Southern Indian Ocean (ODP Leg 183, Site 1138). *Proceedings of the Ocean Drilling Program, 183 Scientific Results*. doi:10.2973/odp.proc.sr.183.008.2002

Naafs, B. D. A., & Pancost, R. D. (2016). Sea-surface temperature evolution across Aptian Oceanic Anoxic Event 1a. *Geology*, 44(11), 959–962. doi:10.1130/g38575.1

Naafs, B. D. A., Rohrssen, M., Inglis, G. N., Lähteenoja, O., Feakins, S. J., Collinson, M. E., et al. (2018). High temperatures in the terrestrial mid-latitudes during the early Palaeogene. *Nature Geoscience*, 11(10), 766–771. doi:10.1038/s41561-018-0199-0

NOAA. (2013). *NOAA/NESDIS Geo-polar blended 5 km SST analysis for the full globe*. Office of Satellite and Product Operations. (https://www.ospo.noaa.gov/data/sst/contour/global.fc.gif)

Norris, R. D., & Wilson, P. A. (1998). Low-latitude sea-surface temperatures for the mid-Cretaceous and the evolution of planktic foraminifera. *Geology*, *26*(9), 823-826. doi: 10.1130/0091-7613(1998)026<0823:llsstf>2.3.co;2

Norris, R. D., Bice, K. L., Magno, E. A., & Wilson, P. A. (2002). Jiggling the tropical thermostat in the Cretaceous hothouse. *Geology*, *30*(4), 299-302. doi: 10.1130/0091-7613(2002)030<0299:jtttit>2.0.co;2

O'Brien, C. L., Robinson, S. A., Pancost, R. D., Sinninghe Damsté, J. S., Schouten, S., Lunt, D. J., et al. (2017). Cretaceous sea-surface temperature evolution: Constraints from TEX_{86} and planktonic foraminiferal oxygen isotopes. *Earth-Science Reviews*, 172, 224–247. doi:10.1016/j.earscirev.2017.07.012

Pearson, P. N. (2012). Oxygen isotopes in foraminifera: Overview and historical review. *The Paleontological Society Papers*, 18, 1–38. doi:10.1017/S1089332600002539

Pearson, P. N., van Dongen, B. E., Nicholas, C. J., Pancost, R. D., Schouten, S., Singano, J. M., & Wade, B. S. (2007). Stable warm tropical climate through the Eocene Epoch. *Geology*,

35(3), 211. doi:10.1130/g23175a.1

Petrizzo, M. R. (2001). Late Cretaceous planktonic foraminifera from Kerguelen Plateau (ODP Leg 183): new data to improve the Southern Ocean biozonation. *Cretaceous Research*, 22(6), 829–855. doi:10.1006/cres.2001.0290

Pitcher, A., Wuchter, C., Siedenberg, K., Schouten, S., & Sinninghe Damsté, J. S. (2011). Crenarchaeol tracks winter blooms of ammonia-oxidizing Thaumarchaeota in the coastal North Sea. *Limnology and Oceanography*, 56(6), 2308–2318. doi:10.4319/lo.2011.56.6.2308

Pithan, F., & Mauritsen, T. (2014). Arctic amplification dominated by temperature feedbacks in contemporary climate models. *Nature Geoscience*, 7(3), 181–184. doi:10.1038/ngeo2071

Poulsen, C. J., Barron, E. J., Peterson, W. H., & Wilson, P. A. (1999). A reinterpretation of Mid-Cretaceous shallow marine temperatures through model-data comparison. *Paleoceanography*, 14(6), 679–697. doi:10.1029/1999pa900034

Price, G. (1999). The evidence and implications of polar ice during the Mesozoic. *Earth-Science Reviews, 48*(3), 183–210. doi:10.1016/s0012-8252(99)00048-3

Richey, J. N., Hollander, D. J., Flower, B. P., & Eglinton, T. I. (2011). Merging late Holocene molecular organic and foraminiferal-based geochemical records of sea surface temperature in the Gulf of Mexico. *Paleoceanography*, 26(1). doi:10.1029/2010pa002000

Robert, C., & Maillot, H. (1983). Paleoenvironmental Significance of Clay Mineralogical and Geochemical Data, Southwest Atlantic, Deep Sea Drilling Project Legs 36 and 71. *In* Ludwig, W. J., Krasheninikov, V. A., et al., *Initial Reports of the Deep Sea Drilling Project,* 71: Washington (U.S. Govt. Printing Office). doi:10.2973/dsdp.proc.71.111.1983

Robinson, S. A., & Vance, D. (2012). Widespread and synchronous change in deep-ocean

circulation in the North and South Atlantic during the Late Cretaceous. *Paleoceanography*, 27(1). doi:10.1029/2011pa002240

Robinson, S. A., Dickson, A. J., Pain, A., Jenkyns, H. C., O'Brien, C. L., Farnsworth, A., & Lunt, D. J. (2019). Southern Hemisphere sea-surface temperatures during the Cenomanian–Turonian: Implications for the termination of Anoxic Event 2. *Geology.* 47(2), 131-134 doi:10.1130/g45842.1

Robinson, S. A., Murphy, D. P., Vance, D., & Thomas, D. J. (2010). Formation of "Southern Component Water" in the Late Cretaceous: Evidence from Nd-isotopes. *Geology*, 38(10), 871–874. doi:10.1130/g31165.1

Russo, F., 2013. *Calcareous nannofossil revised biostratigraphy of the latest Albian-earliest Campanian time interval (late Cretaceous)*. PhD Thesis, Università degli studi di Milano, Italy. doi:10.13130/russo-fabio_phd2014-02-12

Sagoo, N., Valdes, P., Flecker, R., Gregoire, L.J. (2013). The Early Eocene equable climate problem: can perturbations of climate model parameters identify possible solutions? *Philosophical Transactions of the Royal Society of London A: Mathematical, Physical and Engineering Sciences*, 371, 0123, doi: 10.1098/rsta.2013.0123

Schmidt, G. A., & Shindell, D. T. (2003). Atmospheric composition, radiative forcing, and climate change as a consequence of a massive methane release from gas hydrates. *Paleoceanography*, 18(1). doi:10.1029/2002pa000757

Schouten, S., Hopmans, E. C., & Sinninghe Damsté, J. S. (2004). The effect of maturity and depositional redox conditions on archaeal tetraether lipid palaeothermometry. *Organic Geochemistry*, 35(5), 567–571. doi:10.1016/j.orggeochem.2004.01.012

Schouten, S., Hopmans, E. C., & Sinninghe Damsté, J. S. (2013). The organic geochemistry of glycerol dialkyl glycerol tetraether lipids: A review. *Organic Geochemistry*, 54, 19–61. doi:10.1016/j.orggeochem.2012.09.006

Schouten, S., Hopmans, E. C., Forster, A., van Breugel, Y., Kuypers, M. M., & Sinninghe Damsté, J. S. (2003). Extremely high sea-surface temperatures at low latitudes during the middle Cretaceous as revealed by archaeal membrane lipids. *Geology*, *31*(12), 1069–1072. doi:10.1130/g19876.1

Schouten, S., Hopmans, E. C., Schefuß, E., & Sinninghe Damsté, J. S. (2002). Distributional variations in marine crenarchaeotal membrane lipids: a new tool for reconstructing ancient sea water temperatures? *Earth and Planetary Science Letters*, 204(1-2), 265–274. doi:10.1016/s0012-821x(02)00979-2

Shah, S.R., Mollenhauer, G., Ohkouchi, N., Eglinton, T.I., Pearson, A., 2008. Origins of archaeal tetraether lipids in sediments: Insights from radiocarbon analysis. *Geochimica et Cosmochimica Acta* 72, 4577-4594, doi: 10.1016/j.gca.2008.06.021

Shintani, T., Yamamoto, M., & Chen, M.-T. (2011). Paleoenvironmental changes in the northern South China Sea over the past 28,000 years: A study of TEX_{86}-derived sea surface temperatures and terrestrial biomarkers. *Journal of Asian Earth Sciences*, 40(6), 1221–1229. doi:10.1016/j.jseaes.2010.09.013

Sinninghe Damsté, J. S., Ossebaar, J., Schouten, S., & Verschuren, D. (2012). Distribution of tetraether lipids in the 25-ka sedimentary record of Lake Challa: extracting reliable TEX_{86} and MBT/CBT palaeotemperatures from an equatorial African lake. *Quaternary Science Reviews,* 50, 43–54. doi:10.1016/j.quascirev.2012.07.001

Sinninghe Damsté, J. S., van Bentum, E. C., Reichart, G.-J., Pross, J., & Schouten, S. (2010). A CO_2 decrease-driven cooling and increased latitudinal temperature gradient during the mid-Cretaceous Oceanic Anoxic Event 2. *Earth and Planetary Science Letters*, 293(1–2), 97–103. doi:10.1016/j.epsl.2010.02.027

Sliter, W. V. (1977). Cretaceous Foraminifers from the Southwestern Atlantic Ocean Leg 36, Deep Sea Drilling Project. *In* Barker, P. F., Dalziel, I. W. D., et al., *Initial Reports of the Deep Sea Drilling Project,* 36: Washington (U.S. Govt. Printing Office). doi:10.2973/dsdp.proc.36.110.1977

Sloan, L. C., & Pollard, D. (1998). Polar stratospheric clouds: A high latitude warming mechanism in an ancient greenhouse world. *Geophysical Research Letters*, 25(18), 3517–3520. doi:10.1029/98gl02492

Sluijs, A., Schouten, S., Pagani, M., Woltering, M., Brinkhuis, H., et al. (2006). Subtropical Arctic Ocean temperatures during the Palaeocene/Eocene thermal maximum. *Nature*, 441(7093), 610–613. doi:10.1038/nature04668

Spero, H. J., & Lea, D. W. (1996). Experimental determination of stable isotope variability in Globigerina bulloides: implications for paleoceanographic reconstructions. *Marine Micropaleontology*, 28(3–4), 231–246. doi:10.1016/0377-8398(96)00003-5

Spielhagen, R. F., Werner, K., Sorensen, S. A., Zamelczyk, K., Kandiano, E., Budeus, G., … Hald, M. (2011). Enhanced Modern Heat Transfer to the Arctic by Warm Atlantic Water. *Science*, 331(6016), 450–453. doi:10.1126/science.1197397

Tabor, C. R., Poulsen, C. J., Lunt, D. J., Rosenbloom, N. A., Otto-Bliesner, B. L., Markwick, P. J., et al. (2016). The cause of Late Cretaceous cooling: A multimodel-proxy comparison.

Geology, 44(11), 963–966. doi:10.1130/g38363.1

Thompson, R. W. (1977). Mesozoic Sedimentation on the Eastern Falkland Plateau. *In* Barker, P. F., Dalziel, I. W. D., et al., *Initial Reports of the Deep Sea Drilling Project*, 36: Washington (U.S. Govt. Printing Office). doi:10.2973/dsdp.proc.36.122.1977

Tierney, J. E., & Tingley, M. P. (2014). A Bayesian, spatially-varying calibration model for the TEX_{86} proxy. *Geochimica et Cosmochimica Acta*, 127, 83–106. doi:10.1016/j.gca.2013.11.026

Tierney, J. E., & Tingley, M. P. (2015). A TEX_{86} surface sediment database and extended Bayesian calibration. *Scientific Data*, 2, 150029. doi:10.1038/sdata.2015.29

Ufnar, D. F., González, L. A., Ludvigson, G. A., Brenner, R. L., & Witzke, B. J. (2004). Evidence for increased latent heat transport during the Cretaceous (Albian) greenhouse warming. *Geology, 32*(12), 1049. doi:10.1130/g20828.1

Upchurch, G. R., Kiehl, J., Shields, C., Scherer, J., & Scotese, C. (2015). Latitudinal temperature gradients and high-latitude temperatures during the latest Cretaceous: Congruence of geologic data and climate models. *Geology*, 43(8), 683–686. doi:10.1130/g36802.1

van Helmond, N. A. G. M., Ruvalcaba Baroni, I., Sluijs, A., Sinninghe Damsté, J. S., & Slomp, C. P. (2014). Spatial extent and degree of oxygen depletion in the deep proto-North Atlantic basin during Oceanic Anoxic Event 2. *Geochemistry, Geophysics, Geosystems, 15*(11), 4254–4266. doi:10.1002/2014gc005528

van Helmond, N. A. G. M., Sluijs, A., Sinninghe Damsté, J. S., Reichart, G.-J., Voigt, S., Erbacher, J., et al. (2015). Freshwater discharge controlled deposition of Cenomanian–Turonian black shales on the NW European epicontinental shelf (Wunstorf, northern Germany). *Climate of the Past, 11*(3), 495–508. doi:10.5194/cp-11-495-2015

van Hinsbergen, D. J. J., de Groot, L. V., van Schaik, S. J., Spakman, W., Bijl, P. K., Sluijs, A., et al. (2015). A Paleolatitude Calculator for Paleoclimate Studies. *PLOS ONE*, 10(6), e0126946. doi:10.1371/journal.pone.0126946

Vavrus, S. (2004). The impact of cloud feedbacks on Arctic climate under greenhouse forcing. *Journal of Climate*, *17*(3), 603–615. doi:10.1175/1520-0442(2004)017<0603:TIOCFO>2.0.CO;2

Voigt, S., Gale, A. S., & Flögel, S. (2004). Midlatitude shelf seas in the Cenomanian-Turonian greenhouse world: Temperature evolution and North Atlantic circulation. Paleoceanography, 19(4), n/a–n/a. doi:10.1029/2004pa001015

Wendler, I. (2013). A critical evaluation of carbon isotope stratigraphy and biostratigraphic implications for Late Cretaceous global correlation. *Earth-Science Reviews*, 126, 116–146. doi:10.1016/j.earscirev.2013.08.003

Wilson, P. A., & Norris, R. D. (2001). Warm tropical ocean surface and global anoxia during the mid-Cretaceous period. *Nature*, 412(6845), 425–429. doi:10.1038/35086553

Wilson, P. A., Norris, R. D., & Cooper, M. J. (2002). Testing the Cretaceous greenhouse hypothesis using glassy foraminiferal calcite from the core of the Turonian tropics on Demerara Rise. *Geology*, *30*(7), 607-610. doi: doi.org/10.1130/0091-7613(2002)030<0607:ttcghu>2.0.co;2

Woelders, L., Vellekoop, J., Kroon, D., Smit, J., Casadío, S., Prámparo, M. B., et al. (2017). Latest Cretaceous climatic and environmental change in the South Atlantic region. *Paleoceanography*, 32(5), 466–483. doi:10.1002/2016pa003007.

Woelders, L., Vellekoop, J., Weltje, G. J., de Nooijer, L., Reichart, G.-J., Peterse, F., et al. (2018). Robust multi-proxy data integration, using late Cretaceous paleotemperature records as a

case study. *Earth and Planetary Science Letters*, 500, 215–224. doi:10.1016/j.epsl.2018.08.010.

Wuchter, C., Schouten, S., Wakeham, S. G., & Sinninghe Damsté, J. S. (2005). Temporal and spatial variation in tetraether membrane lipids of marine Crenarchaeota in particulate organic matter: Implications for TEX_{86} paleothermometry. *Paleoceanography*, 20(3). doi:10.1029/2004pa001110

Zachos, J. C., Schouten, S., Bohaty, S., Quattlebaum, T., Sluijs, A., Brinkhuis, H., … Bralower, T. J. (2006). Extreme warming of mid-latitude coastal ocean during the Paleocene-Eocene Thermal Maximum: Inferences from TEX_{86} and isotope data. *Geology*, 34(9), 737–740. doi:10.1130/g22522.1

Zachos, J. C., Stott, L. D., & Lohmann, K. C. (1994). Evolution of Early Cenozoic marine temperatures. *Paleoceanography*, 9(2), 353–387. doi:10.1029/93pa03266

Zhang, Y. G., Pagani, M., & Wang, Z. (2016). Ring Index: A new strategy to evaluate the integrity of TEX_{86} paleothermometry. *Paleoceanography*, 31(2), 220–232. doi:10.1002/2015pa002848

Zhang, Y. G., Zhang, C. L., Liu, X.-L., Li, L., Hinrichs, K.-U., & Noakes, J. E. (2011). Methane Index: A tetraether archaeal lipid biomarker indicator for detecting the instability of marine gas hydrates. *Earth and Planetary Science Letters*, 307(3–4), 525–534. doi:10.1016/j.epsl.2011.05.031

Zhou, J., Poulsen, C. J., Rosenbloom, N., Shields, C., & Briegleb, B. (2012). Vegetation-climate interactions in the warm mid-Cretaceous. *Climate of the Past*, 8(2), 565–576. doi:10.5194/cp-8-565-2012

Figure 1. DSDP/ODP Sites used in this study (stars) and previously published data (circles). Adapted from Blakey 2016.

Figure 2. New TEX_{86} and stable-isotope data generated from DSDP Sites 511 and 327, plotted against depth. For TEX_{86} values, closed circles indicate reliable data and open circles indicate samples with GDGT indices exceeding acceptable thresholds (see supplementary information for details).

Figure 3. New TEX_{86} and stable-isotope data generated from DSDP Sites 511 and 327, plotted against depth.

Figure 4. Compilation of benthic foraminiferal $\delta^{18}O$, bulk carbonate $\delta^{18}O$, planktic foraminiferal $\delta^{18}O$, and TEX_{86} data. All oxygen isotope values are reported VPDB. [1]Huber et al., 2018; [2]Huber et al., 1995; [3]Barrera & Savin, 1999; [4]Friedrich et al., 2009; [5]Barrera & Huber, 1990; [6]Falzoni et al., 2016; [7]Clarke and Jenkyns, 1999; [8]Ando et al., 2013; [9]Woelders et al., 2018; [10]Bice et al., 2003; [11]Forster et al., 2007; [12]Schouten et al., 2003; [13]Bornemann et al., 2008; [14]Sinninghe Damsté et al., 2010; [15]Robinson et al., 2019; [16]Alsenz et al., 2013; [17]van Helmond et al., 2014; [18]Linnert et al., 2014; [19]van Helmond et al., 2015; [20]Woelders et al., 2017. All age models from original sources, plotted on the 2016 timescale. Bulk carbonate and fine-fraction $\delta^{18}O$ values are plotted with the benthic foraminifera d18O values as the carbonate is assumed to have either a bottom-water

diagenetic overprint and/or offsets related to vital effects in the calcareous nannoplankton that contribute much of carbonate to the sediment (e.g. Falzoni et al., 2016).

Figure 5. Photographs of planktic foraminifera showing excellent preservation. Scale = 0.1 mm. a) *A. australis* from Site 511; b) *H. planata* from Site 511; c) *M. marginata* from Site 327; d) *H. globulosa* from Site 327.

Figure 6. A comparison of benthic and upper ocean temperatures at DSDP Site 511, calculated from $\delta^{18}O$ and TEX_{86}. Planktonic foraminifera includes all taxa, irrespective of depth habitat. See text for description of approach used to calculate temperatures from oxygen-isotopes. SSTs were calculated from TEX_{86} using the following empirical calibrations: TEX_{86}^{H} (Kim et al., 2010), TEX_{86}-linear (O'Brien et al., 2017) and the deep-time version of BAYSPAR (Tierney and Tingley, 2014, 2015). Age model from Huber et al. (2018).